Photoacoustic Spectroscopy in Trace Gas Monitoring

Frans J.M. Harren, Gina Cotti, Jos Oomens, and Sacco te Lintel Hekkert

in
Encyclopedia of Analytical Chemistry
R.A. Meyers (Ed.)
pp. 2203–2226

Photoacoustic Spectroscopy in Trace Gas Monitoring

Frans J.M. Harren, Gina Cotti, Jos Oomens, and Sacco te Lintel Hekkert
University of Nijmegen, The Netherlands

Since ancient times people have searched for ways to understand processes occurring in the environment, atmosphere or living organisms. Study of the gaseous trace compounds present may shed new light on chemical reactions taking place in the atmosphere or biochemical reactions inside organisms such as plants, animals and human beings. This article presents photoacoustic spectroscopy as a sensitive, on-line and noninvasive tool for monitoring the concentration of trace gases. Following a short introduction and a historic overview, attention is focused on the description of devices and equipment which determine the detection limits and selectivity. An overview is given of the current detection limits for photoacoustic detection. Applications are discussed with emphasis on environmental monitoring (in ambient air, car exhaust and stack gas emission), on medical applications and on biological applications (in postharvest physiology, plant physiology, microbiology and entomology).

1 INTRODUCTION

A gaseous molecule that absorbs electromagnetic radiation is excited to a higher electronic, vibrational or rotational quantum state. Generally, depopulation of this quantum state to lower lying states occurs either via fluorescence or collisions, the latter giving rise to a temperature increase of the gas due to energy transfer to translation. This nonradiative relaxation process occurs when the relaxation time can compete with the radiative lifetime of the excited energy levels. Radiative decay has a characteristic lifetime of 10^{-7} s at visible wavelengths as compared with 10^{-2} s at 10 μm. For nonradiative decay these values depend on the pressure (decay time τ inversely proportional to the pressure) and can vary strongly at atmospheric pressures (10^{-3}–10^{-8} s).

By modulating the radiation source at an acoustic frequency the temperature changes periodically, giving rise to a periodical pressure change which can be observed as an acoustic signal; in the gas phase the effect can be detected with a sensitive microphone.

Laser-based photoacoustic detectors are able to monitor trace gas concentrations under atmospheric conditions with orders of magnitude better sensitivity than conventional scientific instrumentation; in addition they are able to monitor noninvasively and on-line under dynamic conditions.

2 HISTORY

The photoacoustic effect was first reported by Alexander Graham Bell in 1880;[1] he discovered that thin discs emitted sound when exposed to a rapidly interrupted beam of sunlight. In a later experiment,[2] he removed the eye-piece of a commercial spectroscope and placed absorbing substances at the focal point of the instrument. The substances were put in contact with the ear by means of a hearing tube (Figure 1a and b) and he found "good" sounds in all parts of the visible and invisible electromagnetic spectrum of the sun.

Other publications on this phenomenon followed this first work; we mention here the works of Röntgen,[3] Tyndall[4] and Preece.[5] However, due to the lack of a quantitative description and the lack of a sensitive microphone, interest in the photoacoustic effect soon declined.

In 1938 Viegerov refined the photoacoustic technique for the first spectroscopic gas analysis;[6] hereafter Luft[7]

Encyclopedia of Analytical Chemistry

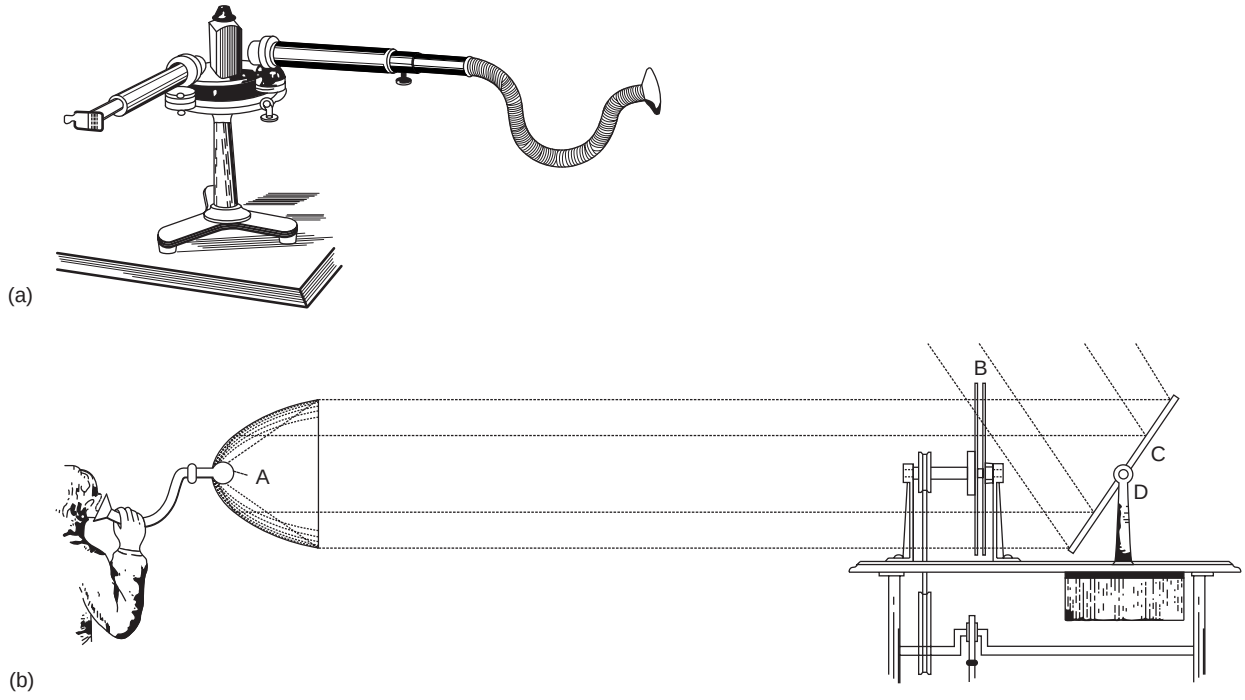

Figure 1 (a) The eye piece of a spectroscope is removed and substances are placed in the focal point of the instrument behind a slit. These substances are put in contact with the ear by means of a hearing tube.[2] (b) Sunlight is intercepted and aligned with a steering mirror (C, D), modulated with a chopper (B) and focused onto a glass bulb (A).[2]

measured trace gas absorption spectra with an infrared broadband light source down to the parts per million level.

By the end of the 1960s, after the invention of the laser, scientific interest increased once again. In 1968, Kerr and Atwood[8] utilized laser photoacoustic detection to obtain the absorption spectrum of small gaseous molecules. Due to the high spectral brightness of lasers and improved phase-sensitive lock-in techniques that amplified the acoustic signal, they were able to determine low concentrations of air pollutants. Kreuzer[9] demonstrated that it was possible to detect concentrations of e.g. 10^{-8} (10 parts per billion) of methane in nitrogen, using an intensity modulated infrared (3 μm) He-Ne laser. Patel et al. demonstrated the potential of the technique by measuring the NO and H_2O concentrations at an altitude of 28 km with a balloon-borne spin-flip Raman laser.[10] After this the photoacoustic effect was introduced into the field of trace gas detection with environmental, biological and medical applications.

3 DEVICES AND EQUIPMENT

3.1 Light Sources

With reference to the previous paragraph, lasers are not essential to operate photoacoustic gas detection systems. Although the spectral power density of broadband infrared light sources is orders of magnitude lower compared with lasers, their advantages are reliability and cost effectiveness. Infrared light sources in combination with various photoacoustic detection schemes are commercially available for trace gas detection at parts per million levels. Spectral selectivity is achieved by using FTIR (Fourier transformed infrared) spectroscopy in combination with spectral band filters in front of the photoacoustic cell; thus typically seven molecular gases can be detected simultaneously at the 1–100 ppm level.

The URAS gas analyzer of Hartmann & Braun uses a photoacoustic detection scheme which is able to detect a specific gas out of a multicomponent gas mixture avoiding cross interferences. In this instrument selectivity is achieved by comparing the direct absorption in a sample cell to that in a reference cell. After passing the sampling cells, each attenuated light beam enters a second detection cell filled only with the gas of interest (Figure 2); the detection cells are interconnected via a membrane connected to a capacitor. Since the dual beam is modulated the difference in acoustic energy reflects the difference in absorption and thus the concentration difference between sample cell and reference cell. The species under investigation enables the wavelength to be selected in such a way that all wavelengths at which absorption occurs are simultaneously active. When there is no spectral overlap from other gases, additional absorptions in the sample cell will not contribute to the acoustic signal; the light passes the

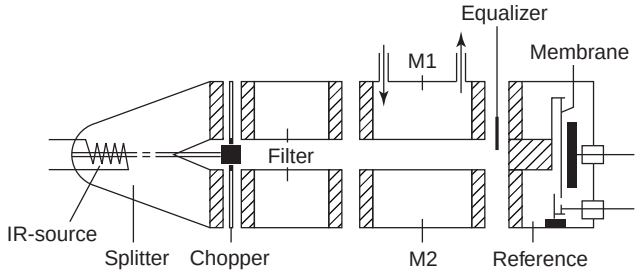

Figure 2 Infrared gas analyzer of Hartmann & Braun with photoacoustic detection scheme to detect a specific gas from a multicomponent gas mixture thereby avoiding cross-interference. Light from the infrared source is split into two paths. The chopper modulates the intensity for both paths. A filter volume in each path serves to filter out light of wavelengths not needed for the detection process; they can be filled with gases whose absorption spectra do not overlap with those of the species under scrutiny. M1 and M2 serve as measuring cell and reference cell respectively. With the help of the equalizer both light intensities become equal before entering the last cell. The last cell consists of two compartments with a membrane between them. Both compartments are filled with the gas under investigation so that all wavelength characteristics for this gas contribute to the signal. If the attenuation differs in M1 from that in M2 the membrane starts to oscillate with the frequency of the chopper. This oscillation (typically a few hertz) is detected capacitively.

detection cell unattenuated. When a specific compound, e.g. H_2O, causes spectral overlap, an extra cell can be placed in the light path filled with the interfering gas. This cell completely attenuates the wavelengths where this interfering molecule absorbs, including the spectral overlap regions. Thus, these wavelengths cannot contribute to the photoacoustic signal and a single component of a complex multicomponent gas mixture can be detected.

High spectral brightness renders CW (continuous wave) laser sources ideally suitable for photoacoustic trace gas detection. In contrast to direct absorption techniques, the photoacoustic signal is proportional to the laser power; from the Lambert–Beer law one finds for small absorptions (Equation 1)

$$P = P_0 e^{-\sigma N l} \longrightarrow (P_0 - P) \approx P_0 \sigma N l \qquad (1)$$

where P_0 and P are the laser power before and after the photoacoustic cell, respectively, σ is the absorption cross-section per molecule (in cm^2), N is the number of absorbing molecules per cubic centimeters and l the absorption path length (in cm). The absorbed energy $(P_0 - P)$ is converted into acoustic energy which is recorded by the microphone.

Saturation, due to nonlinear absorption of the laser power only occurs in focused high-power laser beams. The pumping rate to a higher rovibrational level is proportional to the laser light intensity; in the case of saturation it exceeds the collisional de-excitation rates.

Besides sensitivity, lasers achieve high selectivity. The spectral selectivity is only limited by the pressure broadened absorption profiles of the gases under investigation. The first practical lasers which were used to detect trace gases were CO_2 lasers.[11] These line tunable lasers cover the infrared 9–11 μm wavelength region with a laser line spacing of 0.5–2 cm^{-1}. Fingerprint absorption spectra can be achieved if we compare the laser line spacing to the pressure broadened absorption lines for the trace gas molecules (typically a few gigahertz at atmospheric pressures). Additionally, they are able to deliver high laser powers (1–100 W) from a relatively small gas discharge tube.

A new development is the application of the CO laser in its $\Delta v = 1$ (5.0–7.6 μm wavelength region) and $\Delta v = 2$ (2.5–3.8 μm) version. Although less powerful (typically 1 W) its performance can be improved by applying an intracavity set-up. CO lasers are line tunable with a line spacing between 0.5–1 cm^{-1}.

Other CW lasers in the visible and infrared have been applied to photoacoustic trace gas detection such as a spin flip Raman laser,[10] diode lasers[12,13] and dye lasers.[14] Although dye lasers and titanium sapphire do not cover the ideal wavelength region for trace gas detection they are very well suited for photoacoustic spectroscopy of weak absorption bands with their continuous tunability and a typical CW laser power of 1 W and they have proved their potential in molecular spectroscopy of highly vibrationally excited molecules.[15,16] However, for trace gas detection they are less applicable since the overtone molecular absorption cross-sections are weak, thereby raising the detection limits. For the same reason infrared diode lasers derived from telecommunication research (0.8 and 1.5 μm) are not very well suited.

Of periodically poled nonlinear crystals that have been developed, periodically poled lithium niobate (PPLN) is probably most well known.[17] Lithium niobate ($LiNbO_3$) can be used in combination with pulsed lasers to generate mid-infrared radiation (2–5 μm) by parametric oscillation. CW operation was limited to a few microwatts of laser power due to phase matching problems. Quasi-phase matching with periodically poled materials overcomes this problem resulting in laser powers up to a few watts in the infrared.[18]

The advantage of using pulsed lasers for photoacoustic detection is their wider infrared tunability and consequently better spectral overlap with interesting molecular gases. Examples can be given of the experiments performed with a pulsed CO_2 laser by Repond and Sigrist[19] and experiments with a pulsed optical parametric oscillator (OPO).[20] A disadvantage of pulsed lasers is their high peak powers (megawatt) in relation to their relatively low average energy (typically 1 W) which has to generate a relatively slow process as the gas phase photoacoustic

effect. Peak-to-peak fluctuation and nonlinear absorption disturb the reproducibility of the generated signal, thereby raising detection limits. Typical detection limits reported with these types of laser are in the parts per million range.

3.2 Photoacoustic Cells

To perform trace gas detection the ideal photoacoustic cell should amplify the generated sound originating from the molecular gas absorption meanwhile rejecting acoustic (and electric) noise and in-phase infrared absorption from other materials. Interfering gases should be distinguished by spectroscopic or physical methods (see section 3.3)

For gas phase measurements, mainly resonant cells are combined with modulated CW lasers and lock-in amplifiers; pulsed lasers are combined with piezoelectric detectors and boxcars. These selective amplifiers arise from the necessity to lower acoustic and electric noise levels thus improving the signal-to-noise ratio.

Other requirements for photoacoustic cells are a low gas consumption or a fast response; for this the active volume of the cell should be small so that no dilution can take place when the trace gas and its carrier flow through the acoustic cell.

If we consider a nonresonant, cylindrical cell, its performance can be expressed as its efficiency to convert absorbed photon energy into acoustic energy; this cell constant F (Pa cm W^{-1})[21,22] is given by Equation (2)

$$F_{\text{nonresonant}} = \frac{G(\gamma - 1)L}{wV} \tag{2}$$

where L and V are the length and the volume of the cell, respectively, γ is the specific heat constant, $w = 2\pi\nu$ the modulation frequency and G is a geometrical factor in the order of one. Within a nonresonant cell the gas absorption signal is independent of the cell length but inversely proportional to its diameter. However, photoacoustic signals are also generated by infrared window absorption. To reduce these signals inside the cell its length should be as long as possible to spread this locally generated sound over the total cell volume.

For a resonant cell, the above cell constant F must be amplified with the quality factor Q of the generated acoustic resonance, Equation (3)

$$F_{\text{resonant}} = QF_{\text{nonresonant}} \tag{3}$$

where Q is expressed by the ratio of the energy stored in the acoustical standing wave divided by the energy losses per cycle. This acoustical amplification process is limited by various dissipation processes which can be divided into surface and volume effects. Main surface losses are viscous and thermal losses at the resonator surface, microphone losses and acoustic wave scattering losses at obstacles in the cell. Volumetric losses are not as important as surface losses and are mainly due to free space viscous and thermal losses and $V-V$, $V-R$, $V-T$ relaxation losses of polyatomic gases.[23]

A cylindrical cavity can be a resonant cavity for sound waves. The resonance frequencies of such a cavity are given by Equation (4)

$$f_{mnp} = v_s \left(\left(\frac{\alpha_{mn}}{2R} \right)^2 + \left(\frac{p}{2L} \right)^2 \right)^{1/2} \tag{4}$$

where v_s is the sound velocity in the gas filling the cavity, R is the radius of the resonator, L is the length, $p = 0, 1, 2, 3 \ldots$ axial mode numbers and α_{mn} is a suitable solution of Bessel equations with $m =$ radial mode number and $n =$ azimuthal mode number (Figure 3).[24]

The cell constant F for all types of cylindrical resonant cells is proportional to $L^{1/2}/R$.[25] Due to their larger diameters resonances in the radial or azimuthal acoustic mode have high Q values and high resonance frequencies but low F values. A longitudinally excited resonator will have a low Q value but, due to its small diameter, a high F value.

In order to obtain an optimum signal-to-noise ratio, noise control and interfering signals have to be taken into account. Theoretically, the ultimately lowest acoustical noise results from random density fluctuations, i.e. Brownian motion, in the gas which is distributed over all frequencies in the sound spectrum. The total power of these density fluctuations is constant, but the frequency distribution is dependent upon local resonances and their Q values. Therefore, using a resonant cell the signal-to-noise ratio will not be improved by considering only these random thermal noise fluctuations.

However, these noise levels are far below other noise sources such as amplifier noise and acoustic disturbances from outside the cell. The power of the amplifier noise varies as $1/f$, where f is the modulation frequency of the light beam. Therefore, in contrast to Brownian noise, it is more advantageous to operate at a cell resonance to increase the generated acoustical signal above the $1/f$

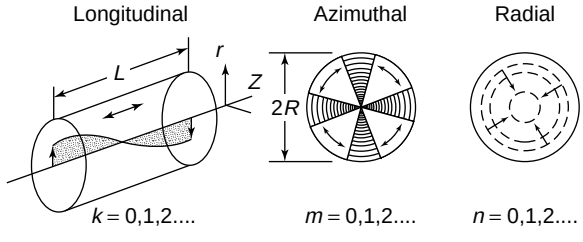

Figure 3 Resonant acoustic modes of a cylindrical closed chamber; the fundamental longitudinal, azimuthal and radial modes.

noise. A prerequisite is that external acoustic disturbances are shielded from the microphone by a proper cell wall construction, material choice and proper design of inlet and outlet ports.

Noise fluctuations do not have a fixed phase relation with the modulation of the light intensity. Other disturbing factors limiting the sensitivity do have a fixed phase relation. Directly generated coherent acoustical background signals, caused by the modulation process (e.g. chopper, current modulation) can be suppressed in the same way as external acoustical disturbances.

Other, more serious interferences are coherent photoacoustic background signals which are caused by absorption of the light beam in the window material or light scattered or reflected off the resonator wall. They are generated at the same frequency and in-phase with the modulated light beam. In resonant cells, window absorption signals can be suppressed by using large buffer volumes and $\lambda/4$-tubes next to the windows.[25] These one-end-open tubes (Figure 4), placed near the window, act as a notch filter for the window signal at the resonance frequency. The influence of the scattered light on the photoacoustic background signal can be minimized by using, for the resonator wall, a highly reflective polished material, with a thermally well conducting material as substrate, e.g. in the case of the CO_2 laser, a polished gold coated copper tube.[26]

In the past special designs have been developed for longitudinally, azimuthally and radially resonant photoacoustic cells,[27–30] even without windows[31,32] to improve sensitivity.

In order to improve the selectivity the combination of the Stark effect or Zeeman effect with photoacoustic detection represents an interesting solution for specific molecules such as ammonia (NH_3)[33,34] and nitric oxide (NO).[35] The change in absorption at a specific laser frequency depends on the shift and splitting of the molecular absorption lines of the species under investigation. Although the method does not suffer from interference problems within multicomponent gas mixtures, there are some limitations. The detection is limited to molecules with a permanent electric or magnetic dipole moment; in addition, the shift or splitting of the lines should be observable within the pressure broadened Lorentzian profile at the overlap with the laser frequency. For ammonia at the 10R8 transition of the $^{12}CO_2$ laser these requirements are satisfied; Thöny and Sigrist[33] showed that the absorption cross-section changed by a factor of two at atmospheric pressure by applying an electric field of 16.7 kV cm^{-1}.

Another way to improve the sensitivity for a specific gas is by temperature change. By increasing the temperature the vapor pressure of, for example, an oil with low vapor pressure is increased thereby improving the sensitivity. An elegant cell has been designed by Jalink and Bicanic,[36] who combined a heatpipe and a photoacoustic cell thereby keeping the microphone and windows at room temperature. In addition, a Helmholtz resonant photoacoustic cell (Figure 5) has been developed by Kästle and Sigrist for quantitative temperature-dependent absorption measurements of fatty acid vapors.[37] Helmholtz resonances (w_H) can be constructed

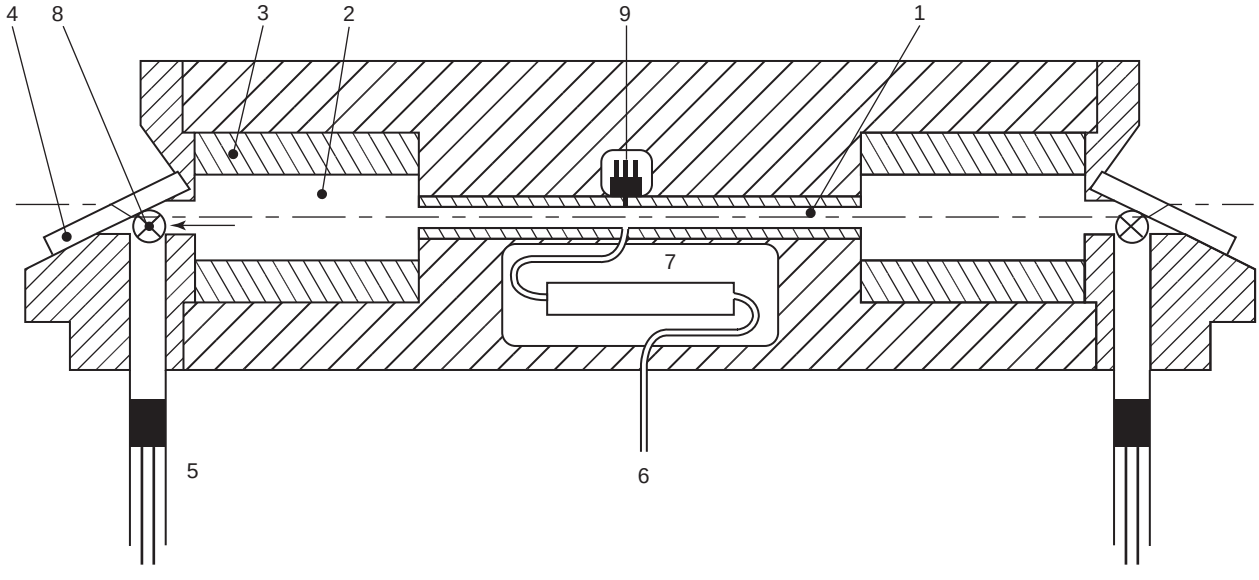

Figure 4 Resonant photoacoustic cell. 1, resonator; 2, buffer volume (maximum diameter 40 mm, length 50 mm); 3, buffer ring to decrease buffer radius; 4, ZnSe Brewster window; 5, adjustable $\lambda/4$ notch filter to suppress window signal; 6, inlet gas flow; 7, $\lambda/2$ notch filter to suppress flow noise; 8, outlet gas flow; 9, Knowless microphone.

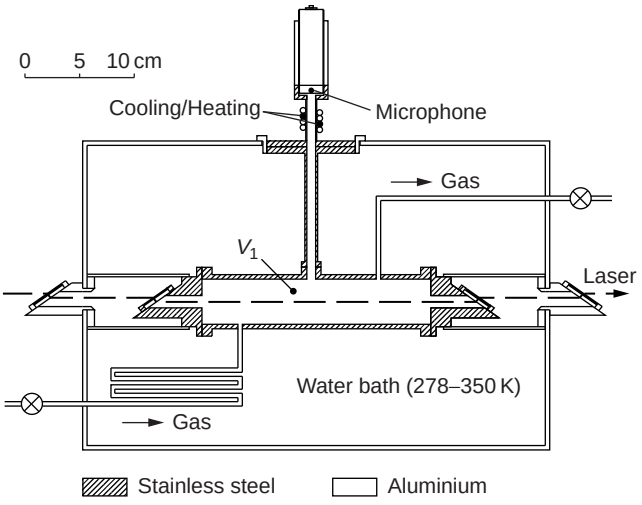

Figure 5 Photoacoustic cell applied for temperature-dependent investigations on fatty acids. The temperature of the water bath was varied between 278 and 350 K with a cold finger and two immersion heaters, while the temperature of the microphone was kept constant with a cooling/heating device. (Reproduced with permission from Kästle and Sigrist, *Appl. Phys. B*, **63**, 389–397 (1996), Copyright Springer Verlag.)

using a relatively large closed volume (V) connected to the outer world via a relatively long narrow duct (length L, cross-section S at a sound velocity c) Equation (5):[24]

$$w_{\mathrm{H}} = \sqrt{\frac{c^2 S}{LV}} \tag{5}$$

Amplification of sound waves can also be achieved with the thermoacoustic effect. The operating principle of such an amplifier connected to a photoacoustic resonator can be explained as follows. The gas inside the acoustical resonator is irradiated by an amplitude modulated laser beam. Trace gas absorption inside the resonator tube will produce a standing acoustical wave; this is the acoustic effect. The amplifier consists of a temperature gradient over a stack of thin sheets separated by a distance equal to two times the thermal boundary layer of the gas (Figure 6). If the gas is moving up and down over the temperature gradient inside the stack, heat energy is transferred to the gas and subsequently into the acoustic standing wave. With such a cell, Q values have been improved by a factor of 20–30.[38] By adjusting the amplifier just below the onset of self-oscillation, the acoustical wave in the resonator will put the amplifier in sustained oscillation, leading to a considerable enhancement of the photoacoustic signal. Noise, acoustic and photoacoustic background signals will also be enhanced. However, with careful design of the cell these levels can be suppressed thereby improving the signal-to-noise ratio.

3.3 Limitations, Selectivity, Interference, Detection Limits

Amplifying photoacoustic signals in resonant cells, reducing noise, using high laser powers, and so on are all used to gain an as high as possible sensitivity for molecular gas absorption. The sensitivity to trace a specific compound depends strongly on its spectroscopic properties. For example, closely spaced rotational absorption lines within a Q branch of a strong vibrational transition help to reach low detection limits of such a gas. One good example is the Q branch of the ν_7 band of C_2H_4 in the 10 μm region. The 10P14 CO_2 laser line is in exact resonance with this Q branch. This results in an extremely low detection limit for C_2H_4 of 6 parts per trillion (1 ppt = 1×10^{12}) in nitrogen. Some gases can be detected even better (e.g. SF_6) while others have higher limits due to less coincidence between available laser frequencies and molecular absorption features. In the future this problem may be overcome by powerful tunable infrared lasers such as the PPLN OPO[39] and quantum cascade lasers.[40] For detection limits see Table 1 and references therein.

Reactive gases such as ozone are very difficult to quantify in absolute concentrations, although ozone has a very strong absorption cross-section in the CO_2 laser wavelength region, resulting in sub-parts per billion detection limits. Ozone is highly reactive, thus interactions with tubing walls, sampling cuvettes, and the photoacoustic cell, cause rapidly decreasing ozone concentrations. This loss in concentration must be determined over the complete sampling system by calibrating the system with a specific ozone analyzer and checked for linearity over a large concentration range. For example, the breakdown of ozone over a 2-m sampling tube may be as high as 60%.[67] The degradation of ozone in a photoacoustic cell is determined to be 75% by inserting a second identical photoacoustic cell in the flow system. In spite of these limitations, successful studies have been performed to quantify atmospheric ozone concentrations.[68]

The first excited vibrational mode of N_2 has a long vibrational lifetime (≈1 ms at 1 atm (1 atm = 101.325 kPa) at $\nu_1 = 2200\,\mathrm{cm}^{-1}$). Using kilohertz modulation of the laser beam a phase shift may occur in the generated photoacoustic signal. A well known example is the kinetic cooling effect of CO_2 at CO_2 laser wavelengths (9–11 μm).[54,69,70] CO_2 has a hot-band absorption in this wavelength region and is excited to the ν_3 vibrational level which is almost resonant with the first vibrational level of N_2. Therefore, under atmospheric conditions the energy absorbed by CO_2 will only slowly be converted into a temperature and pressure increase of the gas.

N_2 is not unique. Another example is given in Figure 7 where CH_4 absorbs the CO laser radiation in

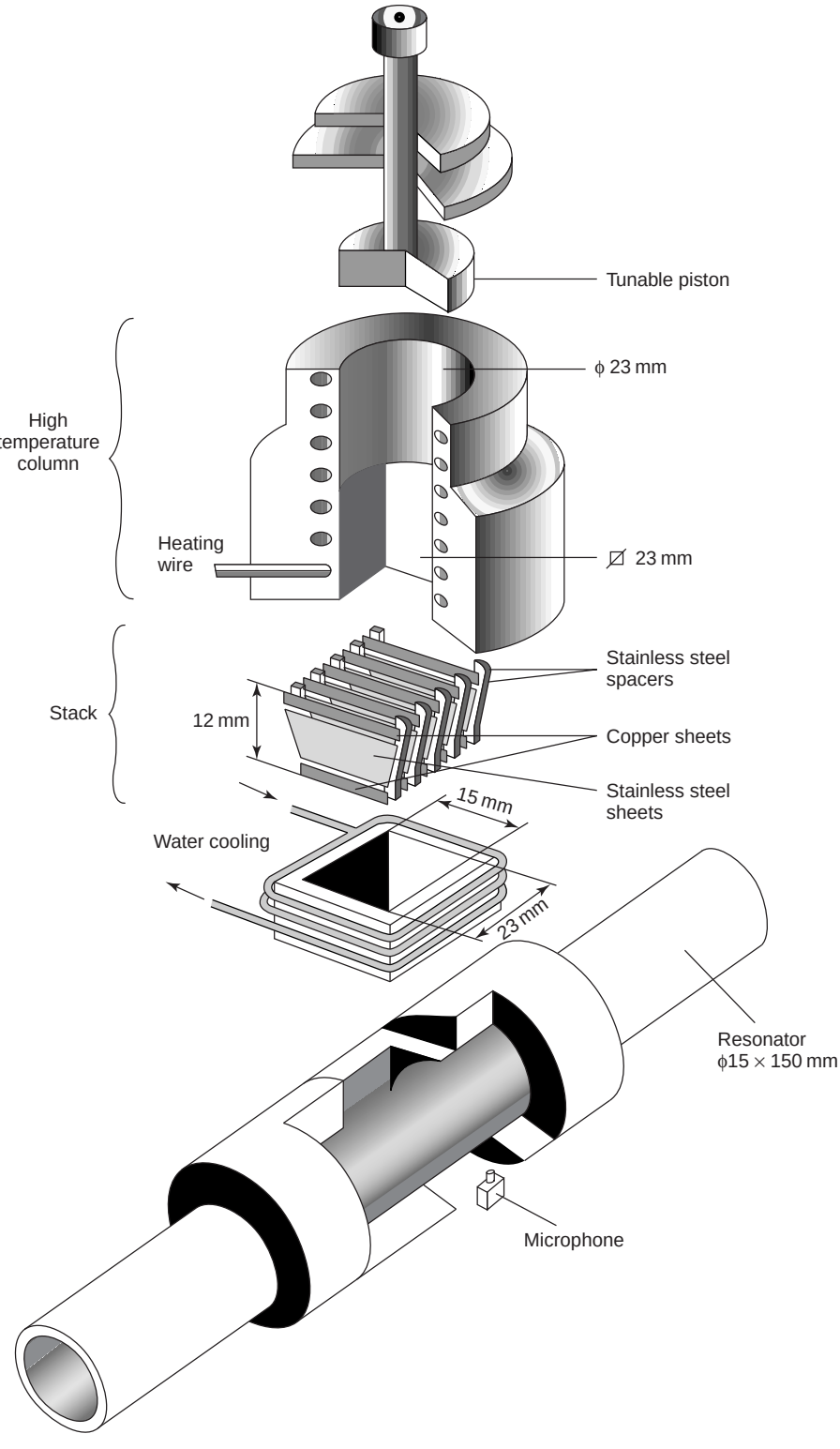

Figure 6 Expanded view of the thermoacoustic stack, dimensions are in millimeters. The tunable piston can slide in the upper part of the column which is cylindrically shaped (diameter 23 mm). The lower part (length 20 mm, square cross-section 23 × 23 mm) forms the connection to the stack. This part is heated by Inconel wire. The exploded view of the stack shows the stainless steel plates with the temperature gradient and copper plates to maintain the gradient; stainless steel spacers separate the plates. At the connection between thermoacoustic stack and the photoacoustic resonator, a water cooler removes the excess heat and keeps the lower end of the stack at constant temperature. (Reproduced with permission from Bijnen et al.)[38]

Table 1 A number of photoacoustic trace gas studies with laser type and molecules investigated[a]

(a) CO lasers

CO laser, 5–6.4 μm[41]a	ppb	CO laser, 5–8 μm[42]	ppb	CO laser[11]	ppb
Nitric oxide	15.4	Carbon disulfide	0.01	Ammonia	0.4
Nitrogen dioxide	0.88	Acetaldehyde	0.1	1,3-Butadiene	1
Nitrous oxide	50	Water vapor	0.1	1-Butadiene	2
Carbon dioxide	5×10^4	Carbon dioxide	1×10^3	Nitric oxide	0.4
Water vapor	65	Nitrogen dioxide	0.1	Nitrous oxide	0.1
Ethylene	42	Nitric oxide	0.3	Propylene	3
Vinyl chloride	10.6	Nitrous oxide	1	Water vapor	14
Propylene	47	Acetylene	1		
1,3-Butadiene	22	Ethylene	1		
Formaldehyde	7.7	Ethane	1		
Acetaldehyde	4.5	Methane	1		
Acrolein	2.1	Pentane	3		
Acetone	4.2	Trimethylamine	1		
Benzene	70	Carbonyl sulfide	1		
Toluene	40	Dimethyl sulfide	3		
m-Xylene	19	Sulfur dioxide	0.1		
o-Xylene	70	Methanethiol	3		
p-Xylene	97	Hydrogen sulfide	100		

(b) Various lasers

Laser	Species	c_{min} (ppb)	Ref.
Dye laser 290–310 nm	Sulfur dioxide	0.12	14
Dye laser 570–620 nm	Nitrogen dioxide	10	43
Dye laser 600 nm	Iodine	260	44
Dye laser 600 nm	Bromine	7.9×10^4	44
HeNe laser 3.39 μm	Methane	10	9
HeNe laser 3.39 μm	C_nH_{2n+2}	10^4–10^5	45
CO Spin flip Raman laser	Nitric oxide	0.1	46
CO laser, Zeeman effect	Nitric oxide	0.01	35
CO laser 4.75 μm	Carbon monoxide	150	47
CO laser 5.40 μm	Phosgene	Few	48
CO laser 5.42 μm	Nitric oxide	0.1–1	45
CO laser 6.13 μm	Nitrogen dioxide	0.01–0.1	45
DF laser 3.87 μm	Methane	1.6×10^3	49
$PbS_{1-x}Se_x$4.8 μm	Carbon monoxide	5×10^4	12
InP/InGaAsP 1.13 μm	Water vapor	1×10^4	13
Diode 10.5 μm	Ethene	200	50

(c) CO_2-lasers

	ppb		ppb
Ref. 51		Ref. 58	
Ethylene	46	Hydrazine	0.2
Benzene	2.05×10^3	Monomethylhydrazine	0.3
Ammonia	35	Unsymmetrical-dimethylhydrazine	0.3
Trichloroethylene	0.55×10^3	Dimethylamine	1.2
Freon-12	0.13×10^3	Trimethylamine	0.3
Ethanol	0.36×10^3	Methanol	0.05
Toluene	0.8×10^3	Ref. 61[b]	
Ref. 52		Acrolein	36
Ethylene	0.02	Styrene	36
Ozone	0.06	Ethyl acrylate	14
Hydrogen sulfide	170	Trichloroethylene	7
1,2-Dibromoethane	0.4	Vinyl bromide	25
Ethyl acetate	0.06	Vinylidene chloride	8

Table 1 (*continued*)

(c) CO_2-lasers (*continued*)

	ppb	Ref.
Ref. 62		
Nitroglycerine	0.28	
Ethylene glycol dinitrate	1.5×10^3	
Dinitrotoluene	16×10^3	
Ref. 63	ppb W^{-1}	
Ethylene glycol dinitrate	8.26	
Nitroglycerine	0.23	
2,4-Dinitrotoluene	0.5	
Cyclohexanone	20.2	
Methylamine	25.3	
Ethylene	0.3	53
Ammonia	1	54[c]
Nitrous oxide	2×10^4	55
Sulfur hexafluoride	0.01	56
Ethylene, Ammonia, Freons, etc.	≤ 4	57
Carbon dioxide	7.4×10^3	31
Ammonia	0.43	31
Ethylene	1.3	31
Ethylene	1–10	45
Ammonia	1–10	45
	Ref. 59[c] 10^{-20} cm^2	Ref. 60[c] ppb
Ethylene	130	0.7
Water vapor	0.005	2×10^4
Propylene	8.2	27
Vinyl chloride	29	2.6
Benzene	7.2	7.2
Toluene	4.5	20
Methanol	72	1.4
Ethanol	17	6
Carbon dioxide	0.015	
1,3-Butadiene	28	
o-Xylene	4.3	
m-Xylene	2.8	
p-Xylene	2.7	
Ethylbenzene	2.3	
Dichloromethane	0.17	
Chlorobenzene	13	
o-Dichlorobenzene	21	
m-Dichlorobenzene	11	
p-Dichlorobenzene	5.5	

	$atm^{-1}cm^{-1}$
Ref. 64	
Sulfur hexafluoride	646
Tungsten hexafluoride	0.091
Uranium hexafluoride	8.5×10^{-4}

	$atm^{-1}cm^{-1}$
Ref. 65	
Acetonenitrile	0.75
Ammonia	69.5
Arsine	5.3
Benzene	2.7
Butadiene	4.4
Ethrane	21.7
Ethylenechlorohydrin	9.3
Ethylene oxide	0.64
	3.4[b]
Formic acid	17.1
Freon-12	99.8
Germane	1.9
Hydrogen selenide	0.5
Perchloroethylene	25.9
Phosgene	1.1
Phosphine	4.0
Styrene	56
	6.0[b]
Sulfur dioxide	0.24
Sulfuryl fluoride	0.19
	53.3[b]
Tricloroethane 111	24.0
Trichloroethylene	15.5
Vinyl chloride	6.6
Ref. 66	
Freon-13	1.24[b]
Freon-22	0.74[b]
Freon-12	79.37[b]
Freon-11	4.23[b]
Ammonia	40.87[b]
Ref. 29	ppb
Acetonitrile	670
Benzene	48
Cyclohexane	250
1,2-Dichloroethane	450
Ethyl acetate	8.3
Freon-12	5.5
Freon-113	5.0
Furan	25
Isopropanol	29
Methylchloroform	11
Methyl ethyl ketone	83
t-Butanol	26
Vinyl chloride	12
Iodopropane	360
Acetylene	3
Ammonia	0.8
Ozone	9
Perchloroethylene	3.2
Trichloroethylene	13

(*continued overleaf*)

Table 1 (*continued*)

(c) CO_2-lasers (*continued*)

	$atm^{-1}cm^{-1}$		$atm^{-1}cm^{-1}$
Sulfur hexafluoride	0.2	Butane	200
1,1-difluoroethylene	5.3	Ethylene glycol dinitrate	38
Freon-11	18	Nitroglycerine	0.7
Freon-114	3.6	Methylamine	120
Ethylene	2.6		

[a] Unless indicated otherwise, detection limits are reported for single-component mixtures with N_2 at 1 atmosphere as buffer gas. Data are given in ppb (1 part per billion volume $= 1 \times 10^9$). In a number of references only absorption strengths are given: σ (in cm^2) or α (in $atm^{-1}cm^{-1}$), with $\alpha = N_{tot} \cdot \sigma$ ($N_{tot} = 2.5 \times 10^{19}$ molecules cm^{-3} at 1013 hPa and 20 °C). When the detection system has a sensitivity of typically $\alpha_{min} = 1 \times 10^{-8}$ the minimum detectable gas concentration can be calculated from $c_{min} = \alpha_{min}/(\sigma \cdot N_{tot})$.
[b] At $^{13}CO_2$ laser lines.
[c] Multicomponent study.

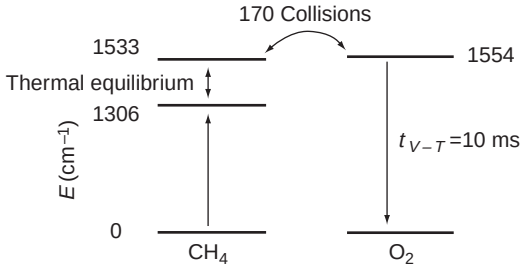

Figure 7 Vibrational energy transfer due to near-resonant energy levels and a slow V–T relexation process, in comparison with the modulation frequency (1010 Hz), may lead to an amplitude decrease and phase shift of the photoacoustic signal. This effect can, for instance, be observed when comparing mixtures of methane in nitrogen and in air, due to rapid vibrational energy transfer between methane and oxygen (see text for details).

the ν_4 vibrational mode centered around 1306.2 cm^{-1}. This is the lowest vibrational mode of the molecule; the collisional relaxation lifetime is therefore large compared with the lifetime of other molecules with a smaller energy gap between their lowest vibrational modes and the ground state. The adjacent ν_2 mode (1533.3 cm^{-1}) becomes thermally populated too (rate constant 13 μs^{-1} atm^{-1}).[71] Oxygen has a near resonant vibrational level (1554 cm^{-1}) and only 170 collisions are needed to transfer energy to the vibrational mode of O_2 (rate constant $\approx$28 μs^{-1} atm^{-1}).[72] Since this is a rather fast process most energy is deposited into O_2 and then relaxes slowly to the ground vibrational state; the average number of collisions required for relaxation to the ground state is 8.3×10^7 in pure O_2 (at standard temperature and pressure 5×10^9 collisions per second take place). The much larger number density of O_2 compared with CH_4 creates a buffer of vibrational energy leading to an effective transient cooling of the translational degrees of freedom. Due to our high modulation frequency (1010 Hz), we observed this transient cooling by O_2 as an amplitude decrease and a phase change relative to the signal caused by the same amount of CH_4 in N_2.

For specific molecules (such as NH_3, NO) spectroscopic interference can be avoided by combining the photoacoustic effect with the Stark or Zeeman effect; the selectivity is enhanced by intermodulating chopper and electric or magnetic fields. A more generally applicable method is to separate gases, either by gas chromatographic methods, selective trapping inside a cold trap,[26] or by a specific chemical reaction (e.g. CO_2 by KOH $\longrightarrow$ K_2CO_3 and water). In most cases, a small amount of the interfering compound remains present. To take this into account, a multicomponent analysis is necessary selecting a number of laser lines on which interfering species and the species of interest have both strong and weak absorptions.

For a multicomponent analysis of a gas mixture, the laser is subsequently tuned to L laser lines. For the analysis it is preferable to obtain an overdetermined system, $G < L$ with G being the number of gases; in this way, more information can be obtained from the gas mixture resulting in more accurate results.[60,73] For practical convenience the background signal generated by window absorption and/or resonator wall absorption is added as a fictive gas component. In the ideal case the measured spectrum is equal to the calculated spectrum. If the absorption coefficient $\sum_{lg}$ of a gas g at laser line l is known, the total absorption at a laser line, α_l is given by Equation (6)

$$\alpha_l = \sum_{g=1}^{G} \Sigma_{lg} \cdot c_g \tag{6}$$

with c_g the concentration of component g. In matrix notation one writes Equation (7)

$$\vec{\alpha} = \vec{\vec{\Sigma}} \cdot \vec{c} \tag{7}$$

If no measurement errors are specified in the absorption coefficient matrix $\vec{\vec{\Sigma}}$ and the measured spectrum ($\tilde{\alpha_l}$), the gas concentration $\vec{c}$ can be calculated by[26] Equation (8)

$$\vec{c} = (\vec{\vec{\Psi}}^{\,t} \cdot \vec{\vec{\Psi}})^{-1} \cdot \vec{\vec{\Psi}}^{\,t} \cdot \vec{1} \tag{8}$$

where $\vec{\vec{\Psi}}^{\,t}$ is the transposed matrix of Ψ_{ij}, $\Psi_{ij} = \sum_{ij} / \alpha_i$ and $1_i = 1$

4 ENVIRONMENTAL APPLICATIONS

4.1 Stack Gas Emission

Several attempts have been made to measure stack gas emissions from power plants. Due to the high amount of nitrogen oxide (NO and NO_2) containing compounds in the emissions, they contribute significantly to photochemical smog formation and acidification of the soil. To reduce the total amount of NO_x in the stack gas, NH_3 is added in the exhaust gas towards the chimney. Using a voluminous catalyst, NO_x reduction within the stack gas takes place. In order to check the performance and to avoid an excess of ammonia injection, the ammonia concentration in the chimney is determined. Olafsson et al. have successfully applied a CO_2 laser-based photoacoustic detection system for in situ monitoring of ammonia concentrations.[74] Due to the difficult hostile environment halfway up the chimney (vibrations, temperature fluctuations, etc.), concessions have to be made as to the sensitivity of the apparatus. With a nonresonant photoacoustic cell at 125 °C, a detection limit of 1 ppm NH_3 was achieved in a multicomponent gas mixture containing 10–15% CO_2.

Gas detection using pulsed lasers in combination with photoacoustic spectroscopy in the UV (ultraviolet) and visible has been developed by Stenberg et al. to analyze gas concentrations in fluidized beds and other combustion environments.[75] The probe has been calibrated for typical combustion gases such as N_2O, NO, NO_2, NH_3, SO_2 and H_2S at temperatures between 20 and 910 °C.

Another example of the potential of the photoacoustic systems to control industrial processes is given by Sigrist[22] who was able to follow the ethanol and methanol emissions from a pharmaceutical production plant with a CO_2 laser-based set-up with a time resolution of 5 min. With this time resolution, strong concentration fluctuations were observed in the exhaust emission, whereas the gas chromatographic system which was used for comparison proved inadequate.

4.2 Car Exhaust Emissions

CO and CO_2 lasers were used to analyze the air polluting emissions from car exhausts. A thorough study was performed by Bernegger and Sigrist to unravel car exhaust mixtures quantifying CO_2, NO and 12 hydrocarbons (see Table 2).[76] To this end, absorption cross-sections of the individual species at each laser line were measured; certified trace gas mixtures in a buffer (mostly N_2) or other certified methods were used to quantify the absolute values. Once the absorption cross-sections are determined, care has to taken to avoid saturation effects (i.e. nonlinearity of the photoacoustic effect with the laser power[52]) and phase shift effects (see previous section). From the absorption cross-sections detection limits can be obtained. In the literature, extremely low detection limits are mentioned based on a signal-to-noise-ratio of one ($S/N = 1$, see Table 1), extrapolated from larger quantities of trace gases in a buffer gas. In reality the detection limits are higher due to multicomponent gas mixtures which induce cross-sensitivities in the absorption coefficients. This mathematical analysis of the photoacoustic spectra is based on the weighted least squares fit of the measured spectra with iteration steps. By choosing the best set of laser lines the error in the calculated concentrations can be reduced.[70,77]

Car exhaust gas mixtures have been investigated by collecting exhaust samples from different motorcycles, diesel and gasoline engines equipped with catalytic converter. The photoacoustic measurements were compared with conventional gas analytical methods. The engine exhaust stream was mixed with air and a fraction of the mixture was collected in a Tedlar sampling bag. Due to the strong water vapor absorption at the CO laser wavelengths and the high water vapor concentrations of 1–2% in the sampling bag, the gas was flowed over a dry-ice cold trap before analysis thereby reducing the water vapor concentration to 0.1%.[76]

4.3 Ambient Air Monitoring

Examples of laboratory photoacoustic studies on multicomponent studies can be found elsewhere.[22] Here we mention two examples of mobile systems which were developed and used in field campaigns. A complete laser photoacoustic system which fitted into two medium sized boxes (0.3 m^3 each) was developed by Rooth et al. to detect ammonia gradients above the heath in the Netherlands.[54] The potential danger of nitrification by NH_3 of such nutrition poor areas motivated the measuring campaign to follow the deposition/emission ratio of ammonia over the area. The system operated for several months, taking data for water vapor, CO_2 (every 40 min) and ammonia (every 6 min).

Another system was developed by Sigrist et al. Installing the whole set-up in a small trailer the stress on the equipment is less severe. Thanks to this approach the system has been operational for years and has been

Table 2 CO laser photoacoustic analyses of vehicle exhausts collected at idling operation of the engine[a] (after Bernegger and Sigrist)[76]

Vehicle	Dried	CO_2(%)	NO	Ethylene	Propylene	Benzene	Toluene	*m*-Xylene	*o*-Xylene	*p*-Xylene	Formal-dehyde	Acetal-dehyde	Acrolein
Volvo (leaded)	Yes	10.3 ± 2.5	105 ± 9	260 ± 20	191 ± 9	37 ± 5	26 ± 14	16 ± 10	42 ± 18	4 ± 19	5.5 ± 1.9	2.7 ± 0.8	2.5 ± 0.4
Jeep	Yes	9.1 ± 1.1	23 ± 2	191 ± 11	109 ± 3	48 ± 3	268 ± 9	67 ± 7	114 ± 10	7 ± 8	1.2 ± 0.6	2.6 ± 0.2	1.2 ± 0.1
(unleaded)	No	11.1 ± 1.3	40 ± 4	206 ± 13	107 ± 5	78 ± 4	196 ± 13	188 ± 12	103 ± 18	67 ± 13	0.1 ± 1.5	4.1 ± 0.3	2.4 ± 0.2
VW Bus	Yes	10.8 ± 1.1	11.8 ± 1.5	172 ± 10	109 ± 4	34 ± 3	149 ± 7	31 ± 7	59 ± 10	2.8 ± 8	0.1 ± 0.8	3.6 ± 0.3	1.7 ± 0.2
(cold catalytic convertor)	No	11.1 ± 1.5	27 ± 3	178 ± 14	98 ± 13	45 ± 5	87 ± 15	39 ± 14	33 ± 19	11 ± 11	1.2 ± 2.6	3.4 ± 0.9	1.9 ± 0.4
Renault Master	Yes	2.8 ± 0.3	10.4 ± 0.9	32 ± 3	18.2 ± 1.2	2.7 ± 0.7	18.5 ± 1.9	4.0 ± 1.7	7.7 ± 2.6	0.5 ± 2.5	8.1 ± 0.8	7.6 ± 0.4	3.2 ± 0.2
(diesel)	No	2.7 ± 0.6	24.5 ± 2.2	33 ± 6	14 ± 8	0.3 ± 2.8	16 ± 7	6.4 ± 6	5.6 ± 10	1.2 ± 6	7.1 ± 2.5	8.7 ± 1.0	4.4 ± 0.5
Unimog	Yes	2.6 ± 0.4	15.7 ± 2.2	5 ± 3	5 ± 2	2.0 ± 0.8	6 ± 2	2.5 ± 2	1 ± 3	5 ± 3	2.6 ± 0.7	2.5 ± 0.3	1.3 ± 0.1
(diesel)	No	2.2 ± 1.0	43 ± 5	7 ± 10	–	–	–	3.5 ± 4	–	8 ± 8	3 ± 7	0.9 ± 2	1.5 ± 1.2
FBW Truck	Yes	1.9 ± 0.4	37 ± 3	16 ± 3	17.5 ± 1.3	–	12 ± 2	1.1 ± 1.5	0.3 ± 3	–	4.2 ± 0.6	7.4 ± 0.2	3.4 ± 0.1
(diesel)	No	2.7 ± 0.9	78 ± 6	23 ± 10	23 ± 9	2 ± 5	20 ± 10	6 ± 7	11 ± 12	3 ± 10	3 ± 2	8.4 ± 0.5	6.9 ± 0.3
Puch motorcycle	Yes	7.9 ± 3	0.3 ± 5	220 ± 10	329 ± 7	203 ± 7	700 ± 20	47 ± 18	135 ± 15	15 ± 10	15.9 ± 1.8	4.1 ± 0.7	6.2 ± 0.3
(2-stroke)	No	8.5 ± 3	0.1 ± 2	234 ± 10	284 ± 7	217 ± 6	405 ± 16	95 ± 13	148 ± 15	20 ± 9	12.6 ± 2.2	5.2 ± 0.8	6.5 ± 0.3

[a] All data are given in parts per million (ppm) with their uncertainty, except for CO_2 (which is in %). The effect of drying of the gas could be observed.

applied in several field campaigns in urban and rural environments.[78] For example, multicomponent gas mixtures were analyzed during sunny days in the summer, using nine laser lines, for the concentration of H_2O, CO_2, NH_3, O_3 and C_2H_4 with a 5 min time resolution.

5 BIOLOGICAL AND MEDICAL APPLICATIONS

5.1 Postharvest Physiology

To delay the effects of aging and ripening, many harvested crops are stored under reduced oxygen concentrations thereby lowering the respiration rate and the rate at which metabolic processes take place. However, when the oxygen concentration falls below a certain limit, crops switch to fermentation, an alternative method to generate the energy needed to sustain their vital functions. This anaerobic metabolism, converts glucose, via several intermediate steps, into acetaldehyde which is then quickly reduced to ethanol. As accumulation of these products in the tissue may affect the quality of the crop, it is necessary to control the rate of fermentation during storage. The concentrations of the volatile in the headspace is an accurate quantitative indicator to assess the rate of fermentation.

Another gas of interest during crop storage is the plant hormone ethylene, which is mainly emitted during ripening of climacteric fruits, i.e. fruits which show a sudden rise in respiratory rate just prior to full ripening. Furthermore, carbon dioxide may be analyzed to assess both respiration and fermentation rates and ethane may be analyzed as the end product of lipid peroxidation causing breakdown of cell membranes.

The noninvasive nature of the photoacoustic trace detection technique renders it extremely suitable for applications in the field of postharvest physiology. Moreover, the high sensitivity combined with fast analysis allows study of an individual piece of fruit so that metabolic activity may be followed in real time. Here we give an overview of some recently performed experiments on single pieces of harvested crops. In general, the crop is placed in a glass container which is connected to the flow-through system leading the released metabolites to the photoacoustic cells. Storage conditions are simulated by supplying the sample with a premixed flow of oxygen and nitrogen (Figure 8); the storage temperature is controlled using a refrigerator.

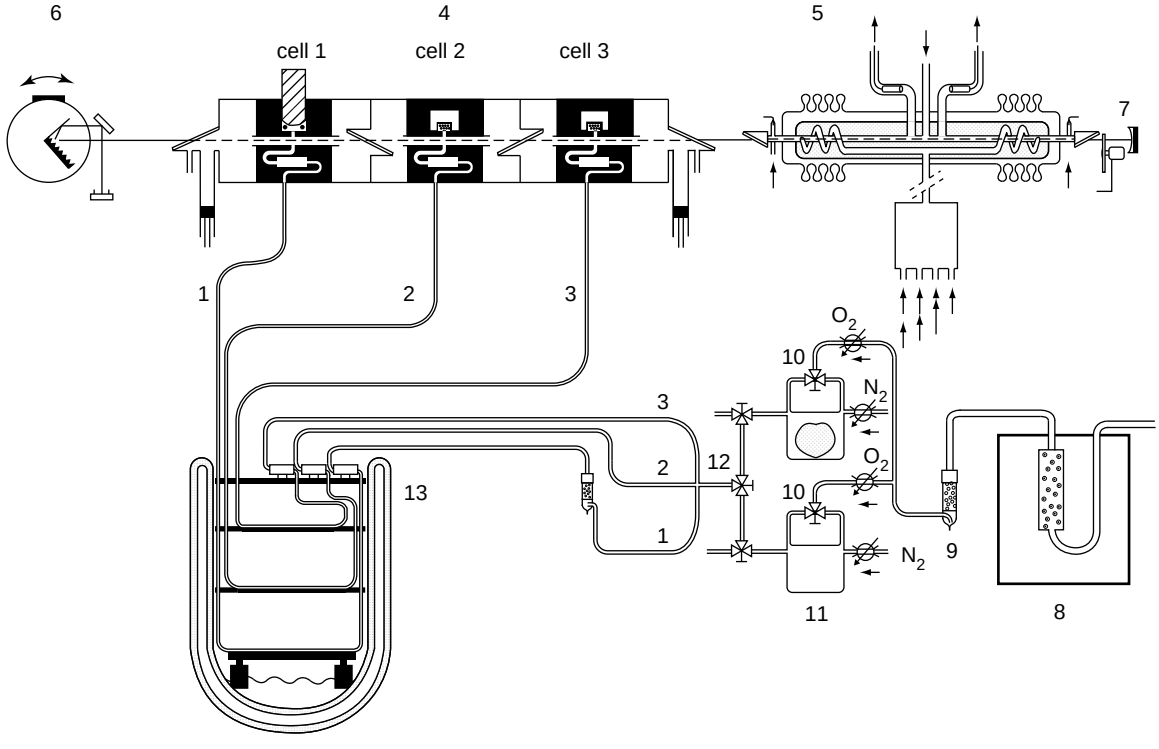

Figure 8 Laser photoacoustic detection set-up. 1, 2 and 3, trace gas flows; 4, triple photoacoustic cell; 5, liquid nitrogen cooled CO laser; 6, grating to select the appropriate transition; 7, chopper; 8, catalyst to remove hydrocarbons from the flow toward the fruit; 9, KOH scrubber to remove CO_2; 10, switching valve for (an)aerobic conditions; 11, cuvettes, one containing a tomato, the other empty as reference; 12, switching valve to select cuvette; 13, cold trap to freeze out interfering gases selectively.

The ethylene emission of climacteric fruit shows a distinct rise during ripening, reaching a maximum when the sample is at its best; subsequent degradation of the product accompanies a decline in the ethylene release. To localize the ethylene release of different crops, De Vries et al. applied the extreme sensitivity of CO_2-laser based photothermal and photoacoustic detectors.[79] Huge differences in emission pathways were found ranging from more than 99% through the skin for banana, apple and citrus fruits, to around 85% through the pedicel "stem" for tomato and bell pepper. In addition, the amount of ethylene released varied from a few tenths to a few thousands of nanoliters per hour per fruit.

When stored crops are returned from controlled atmosphere (CA, low oxygen, high CO_2, low temperature) conditions to normal atmospheric conditions, a rapid peak in the acetaldehyde release occurs due to oxidation of the ethanol accumulated in the tissue. This process was followed in real time for red bell peppers by Zuckermann et al. using a CO laser-based photoacoustic detector.[80] Returning a pepper from anaerobic conditions to normal oxygen conditions (21%) caused a peak in the acetaldehyde release with a maximum of about four times the anaerobic level occurring within 25 min after the switch. The high velocity with which the process takes place caused the authors to conclude that the effect is mainly due to the peroxidative action of the enzyme catalase.[81] Further investigations[82] have shown that the acetaldehyde peak occurs even at much lower postanaerobic O_2 concentrations with roughly equal intensity, though not as fast (Figure 9).

During CA storage of apples it is common practice to apply low concentrations of carbon dioxide externally as it is known to inhibit respiration. As both respiration and fermentation produce carbon dioxide, it is difficult to predict a priori how the fine balance that exists between respiration and fermentation at low O_2 concentrations, will be affected. For pears, at oxygen levels around 1% a substantial rise in the acetaldehyde release could be observed upon addition of a few percent of CO_2. The crop is no longer able to retrieve its energy from respiration and is forced to generate additional energy through fermentation.

5.2 Plant Physiology

One of the major environmental factors influencing crop productivity is flooding. Tolerant species often possess

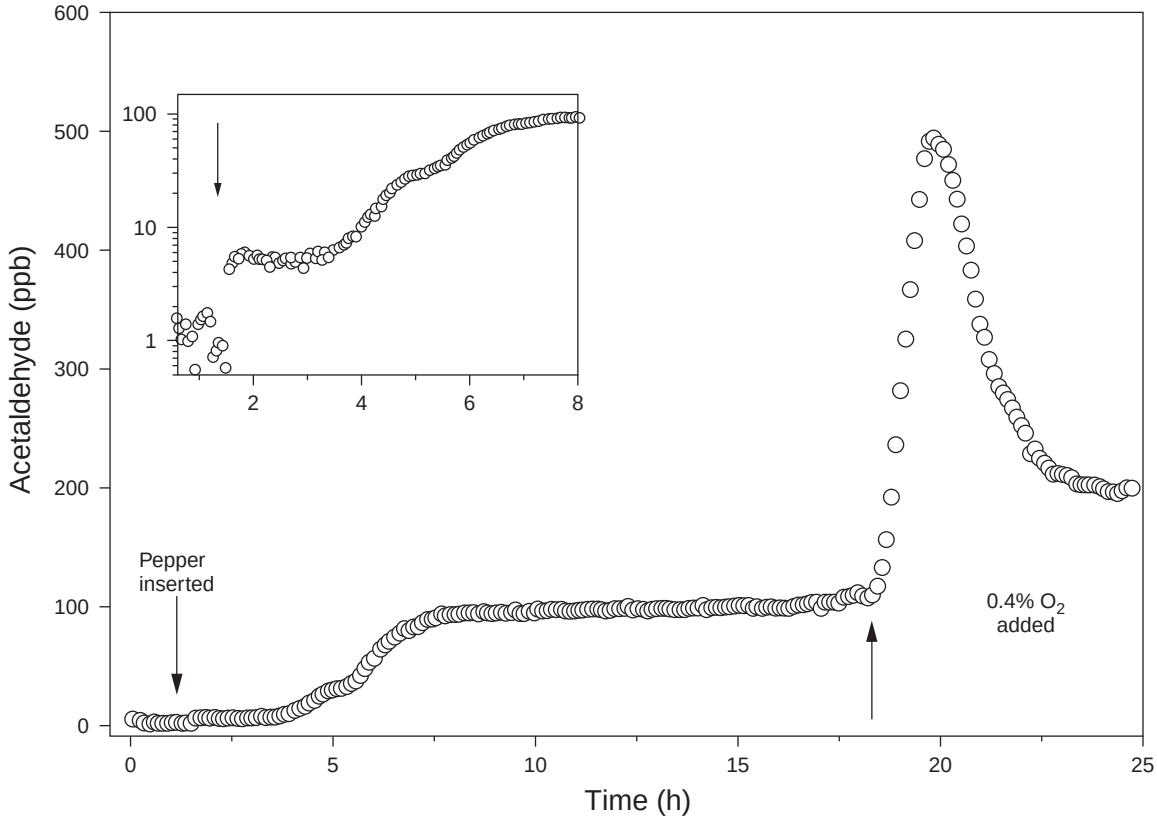

Figure 9 Emission of the precursor of ethanol in the fermentation process, acetaldehyde, is followed on-line while anaerobic conditions are imposed on a red bell pepper. Adding only 0.4% of O_2 results in a strong postanaerobic effect due to the oxidation of ethanol by transient free oxygen radicals in the tissue.

"escape" mechanisms such as fast underwater growth that minimizes the duration of total submergence.[83] However, at early vegetative stages, even in "deep-water" types of rice, such escape is precluded by a lack of sufficiently vigorous shoot elongation for resurfacing. Survival of submergence under these circumstances depends on intrinsic physiological and biochemical tolerance. Screening of cultivars is needed by plant breeders, agrotechnology and biotechnology to achieve sustainable improvements in productivity of rice farming in the rainfed lowland of southeast Asia.[84] Submergence is not an easily quantified stress compared with, for example, cold, heat, or pollution, since it cannot be assessed by one simple analysis. This is because it involves exclusion and entrapment of several key gases and interference with illumination. Normal rates of respiration and photosynthesis are affected; differences in submergence tolerance are also reflected in a different reaction to low oxygen concentrations. Precise measurements of fermentation rates can result in a powerful tool to shed some light on submergence stress. As mentioned in the previous chapter anaerobic fermentation in plant tissue can be studied by use of photoacoustic techniques, through detection of ethanol, acetaldehyde and CO_2 by means of a liquid nitrogen cooled CO laser. Experiments in the laboratory show that seed and seedlings of rice species with different degrees of tolerance toward submergence possess different fermentation rates under anaerobic conditions. Figure 10 shows that after a period of 5 h in which both species have similar ethanol production rates, the most tolerant species (FR13A) starts to slow down fermentation. After about 20 h the production rate for the less tolerant species (CT6241) is doubled with respect to the other; it probably runs out of storage material much faster than the resistant one.

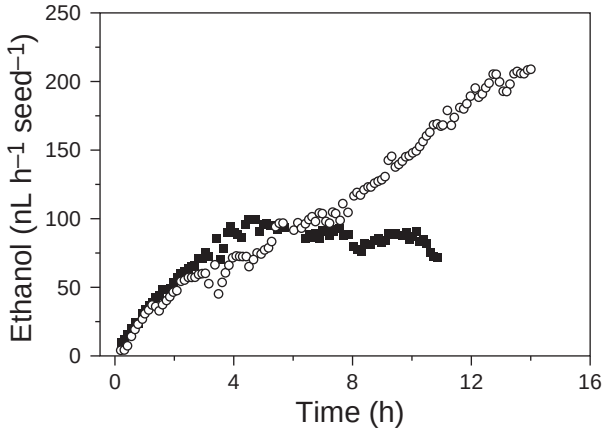

Figure 10 Production rate of ethanol plotted against time for rice seeds during germination under anaerobic conditions. The flooding resistant species (FR13A)(■) does not ferment as much as the intolerant species (CT6241)(○) indicating that it preserves its energy for the postanaerobic period.

Besides fermentation, the availability of oxygen in the roots is of major concern for the plant. In case of partial or complete submergence, rice plants must rely on a well-developed system for gas transport through the plant. The real path of the gas (especially in the shoots) and how this changes with long periods of submergence is unknown. Photoacoustic trace gas detection can also be very useful in this case: a known amount of the tracer gas SF_6 (biologically inactive; atmospheric lifetime 3200 years) is injected into the nutrient solution around the roots and detected coming out of the tip of the leaves, while the rest of the plant is completely submerged in water. We use SF_6 as the tracer gas because the CO_2 laser photoacoustic system is particularly sensitive to this gas (down to parts per trillion level). Figure 11 represents a typical output from the tip of a leaf (enclosed in a cap) after the injection of 4.5 mL of H_2O saturated with SF_6. The plant is kept under water during the experiment.

A question we can readily answer with our system is what kind of gas transport is predominant in the shoots of a young rice seedling. It could be either through aerenchyma (i.e. intercellular spaces present in roots) or through the air layer that is wrapped around the hydrophobic surface of the leaves. This air layer is destroyed by dissolving a few drops of detergent in the water surrounding the plant; because the SF_6 signal dropped to zero immediately afterwards, we can exclude the presence of aerenchyma in the shoots of the seedling.

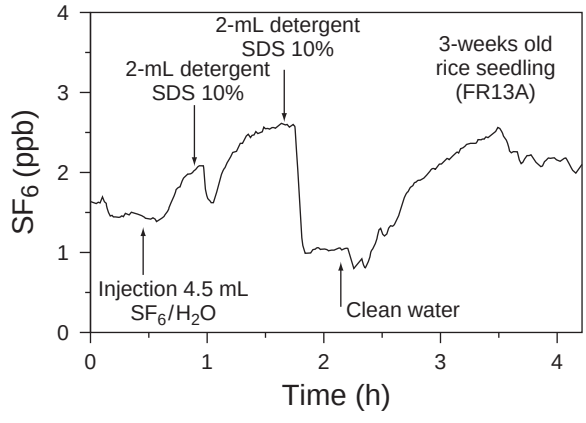

Figure 11 Depletion of the air layer around the submerged rice leaves by addition of detergent. The effect was monitored by SF_6 diffusion which was added into the root compartment (physically separated from the shoot compartment). SF_6 was collected from a small cap filled with air around the tip of a leaf. The air layer is completely restored by replacing the detergent with clean water. During the whole experiment the plant was kept completely submerged.

Another example of trace gas detection within plant physiology is the intriguing question of whether ethylene is a reaction to the growth of the pollen tube inside the pistil (i.e. a form of wounding) or if the pollen tube growth is a consequence of the hormone production by the flower (i.e. a real signal for the plant). It is known that a pollinated flower emits ethylene at the parts per billion level, with a characteristic double peak shaped curve.[85] To answer this question, incongruous pollination has been performed on tobacco flower (*Nicotiana tabacum*), i.e. by pollinating the flower with pollen from other species that show a certain degree of compatibility with the tobacco plant. For this we used pollen with a very low compatibility to the tobacco flower *Nicotiana repanda*; it enters the stigma and stops immediately thereafter. The production of ethylene, detected by photoacoustic spectroscopy, in these cases is very different, as shown in the Figure 12.

The first peak is always reproduced in both height and time and, comparing these results with microscopy work,[86] it corresponds to the entrance of the pollen tube in the stigma. The second peak has a more complicated shape which is never perfectly reproduced with incongruous pollination and which does not simply follow the growth of the pollen tube in the pistil. This might indicate that the second peak is a specific signal from the plant and not a simple wounding effect.

5.3 Microbiology

Biological systems cannot always use molecular nitrogen for their metabolic processes. To this end, dinitrogen

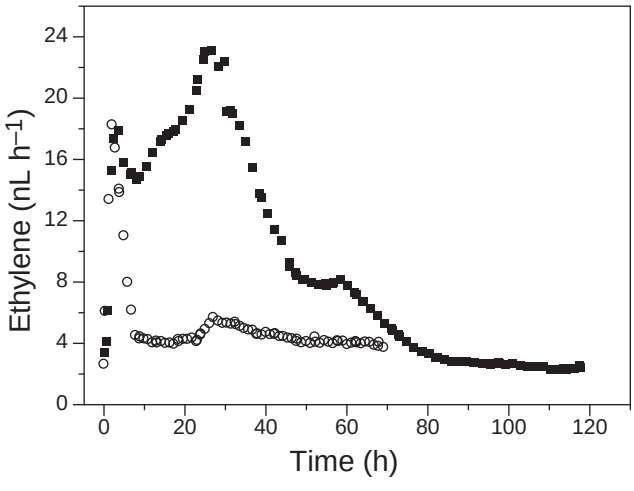

Figure 12 The in vivo production of ethylene during pollination of the *Nicotiana tabacum* flower with two types of pollen: *Nicotiana tabacum* and the incongruous pollen *Nicotiana repanda*. The latter enters the stigma and stops immediately thereafter, whereas the ''right'' pollen grows down the pistil into the ovary for fertilization. ■, *Nicotiana trigonofilla*; ○, *N. repanda*.

(N_2) must be reduced, i.e. the triple bond must be broken to convert the molecule into more appropriate compounds such as ammonium (NH_4^+), nitrate (NO_3^-) or amino acids. Only few organisms are capable of reducing dinitrogen; among them are the diazotrophic cyanobacteria.[87] The nitrogen fixation process is induced by the enzyme nitrogenase, which is very sensitive at low oxygen concentrations. However, like other organisms, cyanobacteria need energy which they derive from photosynthetically produced oxygen. In order to activate both photosynthesis and nitrogen fixation, these processes are separated either in time or in place.[88,89] *Nodularia spumigena* belong to the last category. They consist of large strings of cells formed mainly by vegetative cells in which photosynthesis takes place alternated every 10 to 20 cells by one heterocyst in which the nitrogen fixation takes place.[90]

The acetylene (C_2H_2) reduction method is commonly used to follow the process of nitrogen fixation.[91] As for N_2, the triple bond of acetylene is broken and reduced to ethylene (C_2H_4)[92] which can be detected very sensitively with laser photoacoustics.[52] In the past, gas chromatography utilizing flame ionization detection and photon ionization detection were applied to investigate the nitrogen fixation process.[91,93] Long incubation times, up to several hours, are necessary to reach gas concentrations observable for the equipment making dynamic measurements unfeasible.

Laser photoacoustic experiments have been performed to study the dynamic behavior of nitrogen fixation.[94] To avoid the buffering volume of the water, the algae *Nodularia spumigena* were put on filter paper and a gas mixture of O_2 and N_2 with different concentrations of acetylene was flushed over the sample. In this way the effect of parameters such as light intensity and temperature could be studied with a 20 s time resolution.

Utilizing the CO laser as radiation source instead of the CO_2 laser in the photoacoustic spectrometer, it is possible to detect other interesting gases. Methane and dimethyl sulfide emission in rice field paddies forms an important threat to the environment. Methane is, after CO_2, the second most efficient greenhouse gas whose biological production from the man-made rice cultures, needs further clarification.[95,96] Dimethyl sulfide is a climate-active natural marine emitter and responsible for sulfur transport into the atmosphere. The fact that both gases can be detected very efficiently by photoacoustic techniques, at the water surface as well as at various water depths, forms an important challenge for future activities at field sites.

5.4 Human Health, Noninvasive Breath Analysis

Since ancient times it has been known that the smell of exhaled air can be used as an indicator of several processes

taking place in the human body;[97,98] uncontrolled diabetes produces a sweet fruity odor, advanced liver diseases entail a musty fishy reek, failing kidneys bring about a urine-like smell and a lung abscess can be brought to light by its putrid stench. In the past, several attempts to use trace gas detection of exhaled air have been performed with variable success because of the nonsufficient detection limits of the detectors available. Gases produced in the body are transported to the lungs and are diluted (at rest, healthy persons exhale approximately $1000\,L\,h^{-1}$) before being exhaled. To measure them, it is necessary to enrich the air samples by adsorbing the gases on an agent and releasing the concentrated gas at a certain moment rendering the measurements less accurate and difficult to reproduce.[99]

Measurements on the effects of UV radiation on the human skin are presented to illustrate the possibilities of photoacoustic trace detection in this field. In these experiments lipid peroxidation of the skin is monitored.[100] UV radiation causes reactive oxygen species to be formed in the skin.[101] These radicals can damage the lipids in the cell membranes producing small hydrocarbons such as ethane, pentane and ethylene.[102] With the CO_2 laser set-up it is advantageous to study these latter molecules.[21,52]

A small amount of air is sampled from the exhaled air and cleaned from CO_2 (typically 5%), water vapor and other spectroscopically interfering gases like acetone and ethanol. The test persons are measured while resting under a solar bench. Under UV radiation a steady increase of the exhaled ethylene is observed with a 2 min time delay (Figure 13). The increase continues until the solarium is switched off after 15 min (the maximum exposure time advised). During the subsequent decrease of ethylene emission two decays can be distinguished; a fast and a slow decay. The first decay is caused by the washout of ethylene from the blood; the second decay results from ethylene stored in the body tissue. The dynamics of the system, i.e. transport of gases through the body, yields information for pharmakinetic research. In order to determine the locally induced damage, a specially designed cell was placed on the skin. Immediately after the start of the UV exposure a steady and constant production of ethylene in the skin was observed. Combining the two results, it is concluded that the slow increase in ethylene signal in the exhaled air is caused by the buffering effect of the human body.

Apart from the effect of UV radiation on the skin, other effects induced by lipid peroxidation can be studied: patients suffering from chronic obstructive pulmonary disease have increased cell membrane damage in the lungs; patients with pancreas problems cannot digest long-chain fatty acids, resulting in a lack of ethylene in the exhaled air after consumption of these fatty acids; patients suffering from cardiac insufficiency have increased ethylene levels in the exhaled air.

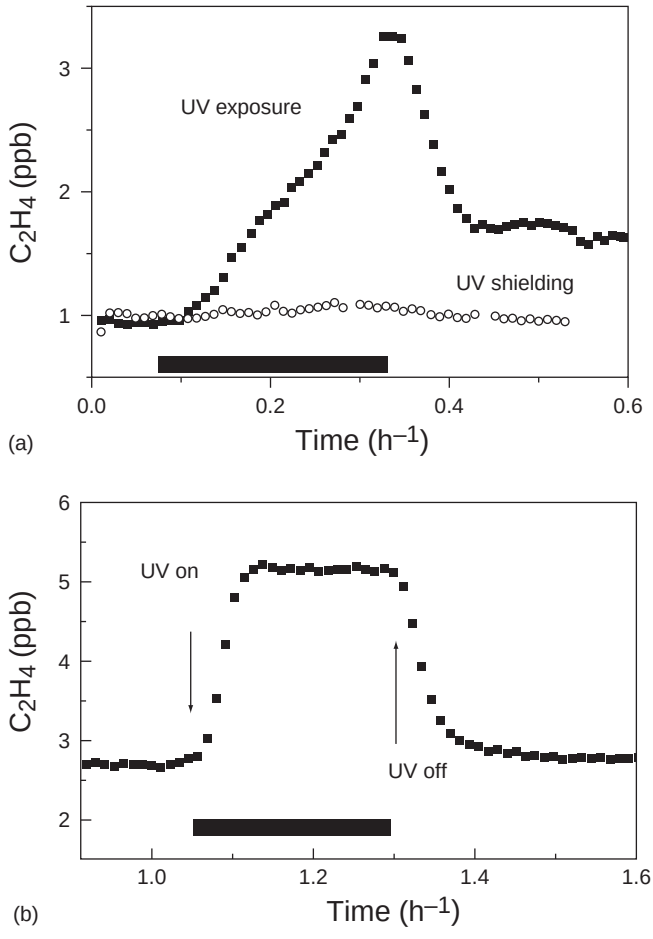

Figure 13 Ethylene emission from the human lungs induced by UV radiation from a solar bench. As a product of lipid peroxidation ethylene is found in low amounts in the exhaled air (a) and directly on the skin (b) utilizing a 5 cm diameter sample cell. The time during which the skin is irradiated (in total 15 min) is indicated by the black bar. Shielding the body from UV radiation using Lexan prevents generation of ethylene.

5.5 Entomology

Methane has been recognized as one of the principal greenhouse gases, second only to CO_2. Its estimated contribution to the enhanced greenhouse effect varies between 15–20% (Intergovernmental Panel on Climate Change, 1990) depending on the time window for which the calculation is made. Methane is not only a potent greenhouse gas, it is also chemically active in the atmosphere thus influencing concentrations of several important species, e.g. OH, O_3 and CO. Biogenic sources are responsible for the major part of the global methane flux (>70%).[103] Some arthropods (i.e. millipedes, cockroaches, termites and scarab beetles)

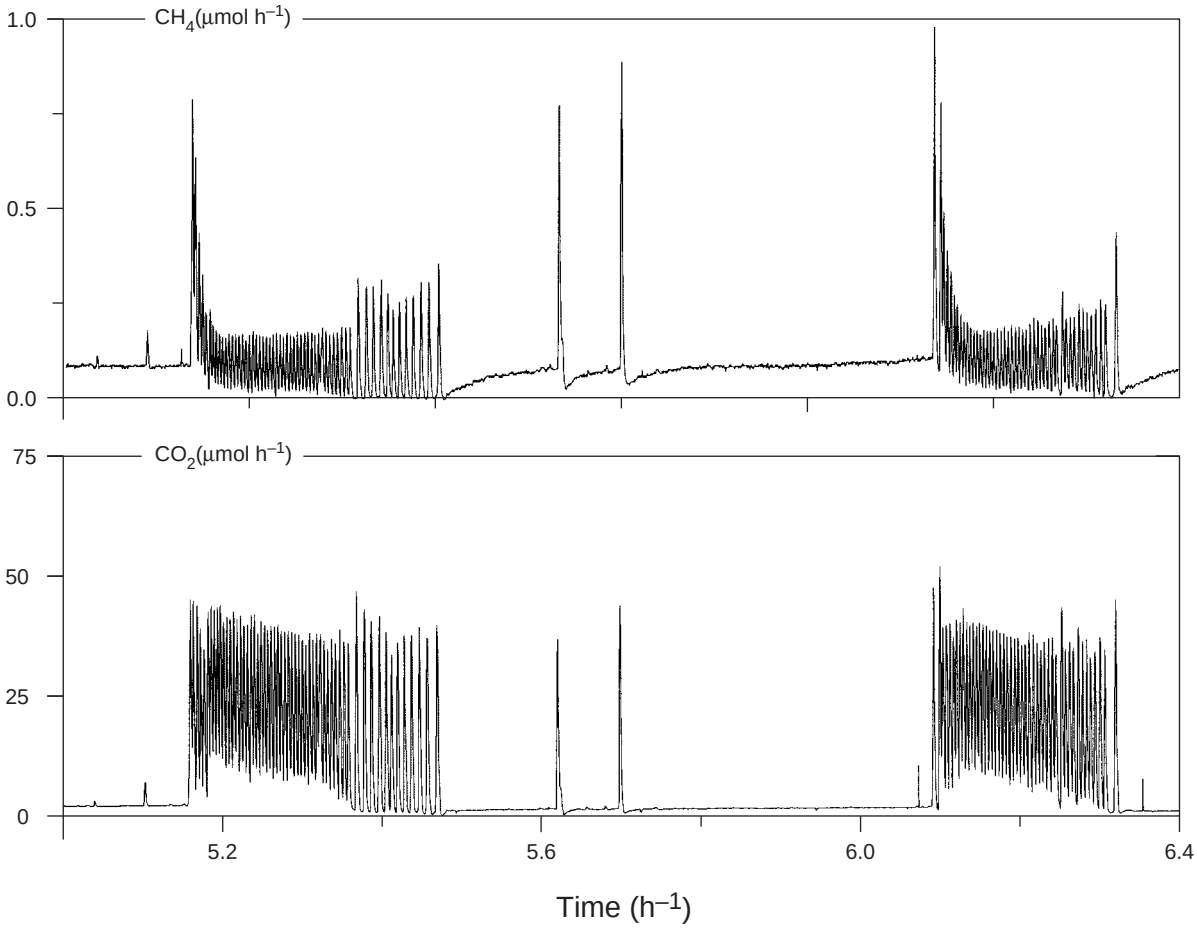

Figure 14 Methane release together with the CO_2 emission, during a complete respiration sequence of breathing (starting at 5.15 h and 6.08 h) and constriction (starting at 5.48 h and 6.32 h) for the cockroach species *Gromphadorhina portentosa*.

are believed to contribute up to 25% of the total budget.[104]

Gas chromatography allows measurement of the methane release of single animals only after incubation for several hours. Consequently these measurements cannot provide information about the dynamic character of the gas emission. Infrared absorption measurements featuring fast response time permitted observation of the dynamics of CO_2 emissions.

Besides CH_4 and CO_2 emissions from insects, water vapor release has been the subject of many studies. Information about water loss dynamics in insects is based upon theoretical modeling, sensitive weighing and relatively slow direct water vapor measurements.[105–108] With laser photoacoustic detection Bijnen et al. showed that cockroaches at rest show a regular breathing pattern that optimizes oxygen uptake and reduces water loss.[26] Respiration patterns of cockroaches and beetles have been recorded where microbiologically produced methane was found to be co-emitted with CO_2 and water vapor (Figure 14). This on-line observation is to be utilized in a study to establish conditions for hyperventilation of insects so that the minimum amount of insecticide will suffice to kill noxious insects which, for example, are known to transmit viral diseases.

6 COMPARISON WITH OTHER SPECTROSCOPIC METHODS IN TRACE GAS MONITORING

Fast and sensitive trace gas detection is not exclusively reserved for photoacoustics. In general, all spectroscopic techniques are able to monitor gas absorptions on a subsecond timescale. However, depending on the type of application not all techniques possess a high sensitivity.

Air pollution can be very well studied with long-path light absorption techniques rendering low detection limits; the sensitivity of the method relies strongly on the path length. A broadband light source (often UV) is directed towards a receiver over an open path in the atmosphere.[22] For stratospheric studies the sun has

also been used as a light source applying a $0.01\,cm^{-1}$ resolution Fourier transform spectrometer on board the space shuttle as part of the Spacelab 3 mission.[109] Laser-based long-path absorption techniques are used either with multipass arrangements, LIDAR (light detection and ranging) or the related DIAL (differential absorption lidar) methods.[22] In contrast to CW operation, using pulsed lasers has the advantage that the backscattered light gives spatial information about the atmospheric absorption pattern.[110]

All methods described above derive their sensitivity from long-path absorption thereby integrating over hundreds of meters. Laser-based photoacoustic detection has the advantage of tracing gases locally and can therefore also be used in laboratory studies. Other laser-based techniques which can also achieve a high sensitivity within a small volume of gas are intracavity laser absorption spectroscopy, which relies on very long effective absorption length within a high optical Q factor laser cavity;[111] cavity ring down spectroscopy combines very accurate decay time measurements of light pulses and a high Q optical cavity resulting in long effective absorption lengths.[112] In comparison with these techniques laser photoacoustics has the advantage that it is background free: it does not rely on a decrease of the transmitted light but on an increase from the zero baseline, i.e. on a collisional release of energy after absorption.

Other background-free and therefore strongly competitive techniques are laser-induced fluorescence (LIF) and multiphoton ionization (MPI). These techniques are both extremely sensitive due to the high collection efficiency of photomultipliers and ion counters; both can be applied locally within a small gas volume. LIF and laser photoacoustics are complementary in energy release. The advantage of LIF is that it can also detect free radicals (e.g. OH) with relatively low laser powers. MPI can be very selective and sensitive for molecules with a higher mass. An elegant example is the detection of OH with LIF in the upper atmospheric layers with an aircraft, avoiding spectroscopic cross interferences from other molecules, laser-induced generation of OH, depletion of OH during sampling, etc.[113] A restriction of LIF is the lifetime of the excited levels. As stated in the introduction, the competition between collisional relaxation and radiative decay restricts LIF mainly to the visible and the UV part of the electromagnetic spectrum.

ACKNOWLEDGMENTS

The authors wish to thank D.H. Parker and J. Reuss for their helpful discussions and continuous support. We are also grateful to H. Zuckermann (Open University of Israel), H.S.M. de Vries, J. Oosterhaven and R.H. Veltman (ATO-DLO) for their collaborations in postharvest research; M.B. Jackson (University of Bristol, UK) for his indispensable contribution in the rice plant research; C. Mariani (University of Nijmegen), D. de Martinis (ENEA, Italy) for their pollination research; M. Staal, L. Stal (NIOO) for their contributions in the field of microbiology; R. Berkelmans, K. Kuiper, P. Hollander (Free University, Amsterdam), P. Scheepers, R. Dekhuijzen (University of Nijmegen) for their help in breath analysis; and P. Kestler (University of Osnabrück, Germany) and J. Hackstein (University of Nijmegen) for their collaborations on entomological applications. Furthermore we thank F. Bijnen, S. Persijn, T. Groot, E. Santosa for their experimental support and C. Sikkens, C. Timmer, H. Schoutissen and L. Gerritsen for technical assistance. Finally we would like to thank the Dutch Technology Foundation (contracts no: NNS44.3404, NNS.4596 and NNS55.3921), the Dutch Royal Academy of Science (contract 95BTM04) and the European Union (contracts no: BRFSCI-CT91-0739, ERB3514-PL95-0708, PL95-0468 and ERB4062-PL970089) for their financial support.

ABBREVIATIONS AND ACRONYMS

CA	Controlled Atmosphere
CW	Continuous Wave
DIAL	Differential Absorption Lidar
FTIR	Fourier Transformed Infrared
LIDAR	Light Detection And Ranging
LIF	Laser-induced Fluorescence
MPI	Multiphoton Ionization
OPO	Optical Parametric Oscillator
PPLN	Periodically Poled Lithium Niobate
UV	Ultraviolet

RELATED ARTICLES

Biomedical Spectroscopy **(Volume 1)**
Biomedical Spectroscopy: Introduction • Infrared Spectroscopy in Microbiology • Infrared Spectroscopy, Ex Vivo Tissue Analysis by

Biomolecules Analysis **(Volume 1)**
Infrared Spectroscopy of Biological Applications

Environment: Trace Gas Monitoring **(Volume 3)**
Environmental Trace Species Monitoring: Introduction • Ultraviolet/Visible Light Detection and Ranging Applications in Air Monitoring

Environment: Water and Waste **(Volume 3)**
Infrared Spectroscopy in Environmental Analysis

Field-portable Instrumentation **(Volume 4)**
Portable Instrumentation: Introduction

Food **(Volume 5)**
Infrared Spectroscopy, Gas Chromatography/Infrared in Food Analysis

Industrial Hygiene **(Volume 6)**
Sensors in the Measurement of Toxic Gases in the Air • Spectroscopic Techniques in Industrial Hygiene

Remote Sensing **(Volume 10)**
Satellite and Sensor Systems for Environmental Monitoring

Atomic Spectroscopy **(Volume 11)**
Laser Spectrometric Techniques in Analytical Atomic Spectrometry

Electronic Absorption and Luminescence **(Volume 12)**
Fluorescence Lifetime Measurements, Applications of

Gas Chromatography **(Volume 12)**
Gas Chromatography: Introduction

Infrared Spectroscopy **(Volume 12)**
Infrared Spectroscopy: Introduction • Gas Chromatography/Infrared Spectroscopy • Quantitative Analysis, Infrared • Theory of Infrared Spectroscopy

General Articles **(Volume 15)**
Quantitative Spectroscopic Calibration

REFERENCES

1. A.G. Bell, 'On the Production and Reproduction of Sound by Light', *Am. J. Sci.*, **XX**, 305–324 (1880).
2. A.G. Bell, 'Upon the Production of Sound by Radiant Energy', *Phil. Mag. J. Sci.*, **XI**, 510–528 (1881).
3. W.C. Röntgen, 'Über Töne, welche durch intermittierende Bestrahlung eines Gases entstehen', *Ann. der Phys. und Chem.*, **1**, 155–159 (1881).
4. J. Tyndall, 'Action of an Intermittent Beam of Radiant Heat upon Gaseous Matter', *Proc. R. Soc.*, **31**, 307–317 (1881).
5. W.H. Preece, 'On the Conversion of Radiant Energy into Sonorous Vibrations', *Proc. R. Soc.*, **31**, 506–520 (1881).
6. M.L. Viegerov, 'Eine Methode der Gasanalyse, Beruhend auf der Optisch-Akustischen Tyndall-Röntgenerscheinung', *Dokl. Akad. Nauk SSSR*, **19**, 687–688 (1938).
7. K.F. Luft, 'Über eine Neue Methode der Registrierenden Gasanalyse mit Hilfe der Absorption Ultraroter Strahlen ohne Spectrale Zerlegung', *Z. Tech. Phys.*, **5**, 97–104 (1943).
8. E.L. Kerr, J.G. Atwood, 'The Laser Illuminated Absorptivity Spectrophone: A Method for Measurement of Weak Absorptivity in Gases at Laser Wavelengths', *Appl. Opt.*, **7**, 915–921 (1968).
9. L.B. Kreuzer, 'Ultralow Gas Concentration Infrared Absorption Spectroscopy', *J. Appl. Phys.*, **42**, 2934–2943 (1971).
10. C.K.N. Patel, E.G. Burkhardt, C.A. Lambert, 'Spectroscopic Measurements of Stratospheric Nitric Oxide and Water Vapor', *Science*, **184**, 1173–1176 (1974).
11. L.B. Kreuzer, N.P. Kenyon, C.K.N. Patel, 'Air Pollution: Sensitive Detection of Ten Pollutant Gases by Carbon Monoxide and Carbon Dioxide Lasers', *Science*, **177**, 347–349 (1972).
12. T.H. Vansteenkiste, F.R. Faxvog, D.M. Roessler, 'Photoacoustic Measurement of Carbon Monoxide Using a Semiconductor Diode Laser', *Appl. Spectrosc.*, **35**, 194–196 (1981).
13. Z. Bozóki, J. Sneider, G. Szabó, A. Miklós, M. Serényi, G. Nagy, M. Fehér, 'Intracavity Photoacoustic Gas Detection With an External Cavity Diode Laser', *Appl. Phys. B*, **63**, 399–401 (1996).
14. K.P. Koch, W. Lahmann, 'Optoacoustic Detection of Sulfur Dioxide below the Parts per Billion Level', *Appl. Phys. Lett.*, **32**, 289–291 (1978).
15. G.J. Scherer, K.K. Lehmann, W. Klemperer, 'The High Resolution Visible Overtone Spectrum of CH_4 and CD_3H at 77 K', *J. Chem. Phys.*, **81**, 5319–5324 (1984).
16. O. Vaittinen, M. Saarinen, L. Halonen, I.M. Mills, 'High Resolution Photoacoustic Overtone Spectroscopy of Monofluoroacetylene, HCCF, with a Titanium : Sapphire Ring Laser', *J. Chem. Phys.*, **99**, 3277–3287 (1993).
17. L.E. Myers, W.R. Bosenberg, 'Periodically Poled Lithium Niobate and Quasi-phase-matched Optical Parametric Oscillators', *IEEE J. Quantum Electron.*, **33**, 1663–1672 (1997).
18. W.R. Bosenberg, A. Drobshoff, J.I. Alexander, L.E. Myers, R.L. Beyer, '93% Pump Depletion, 3.5 W Continuous-wave, Single Resonant Optical Parametric Oscillator', *Opt. Lett.*, **21**, 1336–1338 (1996).
19. Ph. Repond, M.W. Sigrist, 'Photoacoustic Spectroscopy on Trace Gases with a Continuously Tunable CO_2 Laser', *Appl. Opt.*, **35**, 4065–4085 (1996).
20. A. Bohren, M.W. Sigrist, 'Optical Parametric Oscillator Based Difference Frequency Laser Source for Photoacoustic Trace Gas Spectroscopy in the 3 μm mid-IR Range', *Infrared Phys. Technol.*, **38**, 423–435 (1997).
21. Frans Harren, Jörg Reuss, 'Photoacoustic Spectroscopy', in *Encyclopedia of Applied Physics*, ed. G.L. Trigg, VCH, Weinheim, 413–435, Vol. 19, 1997.
22. M.W. Sigrist, *Air Monitoring by Spectroscopic Techniques*, J. Wiley & Sons, New York, 1994.

23. A. Karbach, P. Hess, 'High Precision Acoustic Spectroscopy by Laser Excitation of Resonator Modes', *J. Chem. Phys.*, **83**, 1075–1084 (1985).
24. P.M. Morse, K.U. Ingard, *Theoretical Acoustics*, McGraw-Hill, New York, 1968.
25. F.G.C. Bijnen, J. Reuss, F.J.M. Harren, 'Geometrical Optimization of a Longitudinal Resonant Photoacoustic Cell for Sensitive and Fast Trace Gas Detection', *Rev. Sci. Instrum.*, **67**, 2914–2923 (1996).
26. F.G.C. Bijnen, F.J.M. Harren, J.H.P. Hackstein, J. Reuss, 'Intracavity CO Laser Photoacoustic Trace Gas Detection; Cyclic CH_4, H_2O and CO_2 Emission by Cockroaches and Scarab Beetles', *Appl. Opt.*, **35**, 5357–5368 (1996).
27. R.D. Kamm, 'Detection of Weakly Absorbing Gases Using a Resonant Optoacoustic Method', *J. Appl. Phys.*, **47**, 3550–3558 (1976).
28. A.C. Tam, 'Applications of Photoacoustic Sensing Techniques', *Rev. Mod. Phys.*, **58**, 381–431 (1986).
29. G.A. West, 'Photoacoustic Spectroscopy', *Rev. Sci. Instrum.*, **54**, 797–817 (1983).
30. V.P. Zharov, V.S. Letokhov, *Laser Optoacoustic Spectroscopy*, Springer Verlag, Heidelberg, 1986.
31. G.Z. Angeli, A.M. Solyom, A. Miklos, D.D. Bicanic, 'Calibration of a Windowless Photoacoustic Cell for Detection of Trace Gases', *Anal. Chem.*, **64**, 155–158 (1992).
32. R. Gerlach, N.M. Amer, 'Brewster Window and Windowless Resonant Spectrophones for Intracavity Operation', *Appl. Phys.*, **23**, 319–326 (1980).
33. A. Thöny, M.W. Sigrist, 'Novel Photoacoustic Stark Cell', *Rev. Sci. Instrum.*, **66**, 227–231 (1995).
34. H. Sauren, D. Bicanic, W. Hillen, H. Jalink, C. van Asselt, J. Quist, J. Reuss, 'Resonant Stark Spectrophone as an Enhanced Trace Level Ammonia Concentration Detector: Design and Performance at CO_2 Laser Frequencies', *Appl. Opt.*, **29**, 2679–2682 (1990).
35. M. Seaver, T.J. Manuccia, J.R. McDonald, 'Enhanced Species Selectivity in Opto-acoustic Detection', *Chem. Phys. Lett.*, **123**, 164–168 (1986).
36. H. Jalink, D. Bicanic, 'Concept, Design, and Use of the Photoacoustic Heat Pipe Cell', *Appl. Phys. Lett.*, **55**, 1507–1509 (1989).
37. R. Kästle, M.W. Sigrist, 'Temperature-Dependent Photoacoustic Spectroscopy with a Helmholtz Resonator', *Appl. Phys. B*, **63**, 389–397 (1996).
38. F.G.C. Bijnen, J.V. Dongen, J. Reuss, F.J.M. Harren, 'Thermoacoustic Amplification of Photoacoustic Signal', *Rev. Sci. Instrum.*, **67**, 2317–2324 (1996).
39. F. Kühnemann, K. Schneider, A. Hecker, A. Martis, W. Urban, S. Schiller, J. Mlynek, 'Photoacoustic Trace Gas Detection Using a CW Single Frequency Parametric Oscillator', *Appl. Phys. B*, **66**, 741–745 (1998).
40. J. Faist, F. Capasso, D.L. Sivco, C. Sirtori, A.L. Hutchinson, A.Y. Cho, 'Quantum Cascade Laser', *Science*, **264**, 553–556 (1994).
41. S. Bernegger, 'CO-laser Photoacoustic Spectroscopy of Gases and Vapours for Trace Gas Analysis', Ph.D. Thesis, ETH, Zürich, 1988.
42. S. te Lintel Hekkert, M.J. Staal, R.H.M. Nabben, H. Zuckermann, S. Persijn, L.J. Stal, L.A.C.J. Voesenek, F.J.M. Harren, J. Reuss, D.H. Parker, 'Laser Photoacoustic Trace Gas Detection, an Extremely Sensitive Technique Applied in Biological Research', *Instrum. Sci. Technol.*, **26**, 157–175 (1998).
43. A.M. Angus, E.E. Marinero, J.J. Colles, 'Opto-acoustic Spectroscopy with a Visible CW Dye Laser', *Opt. Commun.*, **14**, 223–225 (1975).
44. R.A. Keller, N.S. Nogar, D.S. Bomse, 'Photoacoustic Detection of Intracavity Absorption', *Appl. Opt.*, **22**, 3331–3334 (1983).
45. A.L. Gandurin, S.B. Gerasimov, A.A. Zheltukhin, I.P. Konovalov, S.T. Kornilov, G.F. Melnik, Y.Y. Mikhalevich, D.D. Ogurok, V.A. Petrishchev, S.N. Chirikov, 'Optoacoustic Gas Analyzer for NO, NO_2, NH_3, C_2H_4, and Saturated Hydrocarbon Pollutants', *Appl. Spectrosc.*, **45**, 886–890 (1987).
46. C.K. Patel, R.J. Kerl, 'A New Optoacoustic Cell with Improved Performance', *Appl. Phys. Lett.*, **30**, 578–579 (1977).
47. R. Gerlach, N.M. Amer, 'Sensitive Optoacoustic Detection of Carbon Monoxide by Resonance Absorption', *Appl. Phys. Lett.*, **32**, 228–231 (1978).
48. X. Luo, F.Y. Shi, J.X. Lin, 'CO-laser Photoacoustic Detection of Phosgene ($COCl_2$)', *Int. J. Infrared Millimeter Waves*, **12**, 141–147 (1991).
49. D.H. Leslie, G.L. Trusty, 'Measurements of DF Laser Absorption by Methane Using an Intracavity Spectrophone', *Appl. Opt.*, **20**, 1941–1947 (1981).
50. F.J.M. Harren, F. Bijnen, C. Liedenbaum, J. Reuss, L.A.C.J. Voesenek, C.W.P.M. Blom, 'Sensitive Photoacoustic Trace Detection of Ethylene', in *Monitoring of Gaseous Pollutants by Tunable Diode Lasers*, eds. R. Grisar, G. Schmidtke, M. Tacke, G. Restelli, Kluwer Academic, Dordrecht, 1989.
51. N. Konjevic, S. Jovicevic, 'Spectrophone Measurements of Air Pollutants Absorption Coefficients at CO_2 Laser Wavelengths', *Spectrosc. Lett.*, **12**, 259–274 (1979).
52. F.J.M. Harren, F.G.C. Bijnen, J. Reuss, L.A.C.J. Voesenek, C.W.P.M. Blom, 'Sensitive Intracavity Photoacoustic Measurements with a CO_2 Waveguide Laser', *Appl. Phys. B*, **50**, 137–144 (1990).
53. E. Kritchman, S. Shtrikman, M. Slatkine, 'Resonant Optoacoustic Cells for Trace Gas Analysis', *J. Opt. Soc. Am.*, **68**, 1257–1271 (1978).
54. R.A. Rooth, A.J.L. Verhage, L.W. Wouters, 'Photoacoustic Measurement of Ammonia in the Atmosphere: Influence of Water Vapor and Carbon Dioxide', *Appl. Opt.*, **29**, 3643–3653 (1990).
55. D.D. Bicanic, A. Bizzarri, B.F.J. Zuidberg, G.P.A. Bot, T. de Jong, H.C.P. Wegh, 'CO_2 Laser Based N_2O Monitor', *Springer Ser. Opt. Sci.*, **58**, 143–144 (1988).

56. E. Nodov, 'Optimization of Resonant Cell Design for Optoacoustic Gas Spectroscopy (H-type)', *Appl. Opt.*, **17**, 1110–1119 (1978).
57. W. Schnell, G. Fischer, 'Carbon Dioxide Laser Absorption Coefficients of Various Air Pollutants', *Appl. Opt.*, **14**, 2058–2059 (1975).
58. G.L. Loper, A.R. Calloway, M.A. Stamps, J.A. Gelbwachs, 'Carbon Dioxide Laser Absorption Spectra and Low ppb Photoacoustic Detection of Hydrazine Fuels', *Appl. Opt.*, **19**, 2726–2734 (1980).
59. P.L. Meyer, M.W. Sigrist, 'Air-pollution Monitoring with a Mobile CO_2 Laser Photoacoustic System', Final Report Swiss National Science Foundation/NFP 14, Project No. 4.684.0.83.14, 1988.
60. P.L. Meyer, M.W. Sigrist, 'Atmospheric Pollution Monitoring Using CO_2-laser Photoacoustic Spectroscopy and Other Techniques', *Rev. Sci. Instrum.*, **61**, 1779–1807 (1990).
61. G.L. Loper, G.R. Sasaki, M.A. Stamps, 'Carbon Dioxide Laser Absorption Spectra of Toxic Industrial Compounds', *Appl. Opt.*, **21**, 1648–1653 (1982).
62. P.C. Claspy, C. Ha, Y.-H. Pao, 'Optoacoustic Detection of NO_2 Using a Pulsed Dye Laser', *Appl. Opt.*, **16**, 2972–2973 (1977).
63. R.A. Crane, 'Laser Optoacoustic Absorption Spectra for Various Explosive Vapours', *Appl. Opt.*, **17**, 2097–2102 (1978).
64. D.M. Cox, A. Gnauck, 'Continuous-wave CO_2 Laser Spectroscopy of SF_6, WF_6, and UF_6', *J. Mol. Spectrosc.*, **81**, 207–215 (1980).
65. M.H. Hubert, J.S. Ryan, R.A. Crane, 'Laser Optoacoustic Detector Measurement of Signatures of a Selection of Environmental Contaminants', Ultra Lasertech Inc., Mississauga, Canada, Rep. No 83-715-1, 1983.
66. Z. Zelinger, I. Jančik, P. Engst, 'Measurement of the NH_3, CCl_2F_2, $CHClF_2$, $CFCl_3$, and $CClF_3$ Absorption Coefficients at Isotopic $^{13}C^{16}O_2$ Laser Wavelengths by Photoacoustic Spectroscopy', *Appl. Opt.*, **31**, 6974–6975 (1992).
67. H.S.M. de Vries, 'Non-intrusive Fruit and Plant Analyses by Laser Photothermal Measurements of Ethylene Emission', in *Fruit and Nut Analyses*, ed. H.F. Linskens, Springer Verlag, Heidelberg, 1–18, 1996.
68. A. Thöny, M.W. Sigrist, 'New Developments in CO_2-laser Photoacoustic Monitoring of Trace Gas', *Infrared Phys. Technol.*, **36**, 585–615 (1995).
69. F.G. Gebhardt, D.C. Smith, 'Kinetic Cooling of a Gas by Absorption of CO_2 Laser Radiation', *Appl. Phys. Lett.*, **20**, 129–132 (1972).
70. M.A. Moeckly, C. Hilbes, M.W. Sigrist, 'Photoacoustic Multicomponent Gas Analysis Using a Levenberg-Marquardt Fit-algorithm', *Appl. Phys. B*, (1998), accepted.
71. E. Avramides, T.F. Hunter, 'Vibrational–Translational/Rotational and Vibrational–Vibrational Processes in Methane: Optoacoustic Measurements', *Chem. Phys.*, **57**, 441–451 (1981).
72. J.D. Lambert, *Vibrational and Rotational Relaxation in Gases*, Clarendon Press, Oxford, 1977.
73. S.B. Tilden, M. Bonner Denton, 'A Comparison of Data Reduction Techniques for Line Excited Optoacoustic Analysis of Mixtures', *Appl. Spectrosc.*, **39**, 1017–1022 (1985).
74. A. Olafsson, M. Hammerich, J. Bülow, J. Henningsen, 'Photoacoustic Detection of NH_3 in Power Plant Emission with a CO_2 Laser', *Appl. Phys. B*, **49**, 91–97 (1989).
75. J. Stenberg, R. Hernberg, J. Vattulainen, 'Analysis of Pollutant Chemistry in Combustion by in situ Pulsed Photoacoustic Laser Diagnostics', *Appl. Opt.*, **34**, 8400–8408 (1995).
76. S. Bernegger, M.W. Sigrist, 'CO-laser Photoacoustic Spectroscopy of Gases and Vapours for Trace Gas Analysis', *Infrared Phys.*, **30**, 375–429 (1990).
77. F.G.C. Bijnen, H. Zuckermann, F.J.M. Harren, J. Reuss, 'Multi-component Trace Gas Analysis by Three Intracavity Photoacoustic Cells in a CO-laser: Observation of Anaerobic and Post Anaerobic Emission of Acetaldehyde and Ethanol in Cherry Tomatoes', *Appl. Opt.*, **37**, 3345–3354 (1998).
78. M.A. Moeckli, M. Fierz, M.W. Sigrist, 'Emission Factors for Ethene and Ammonia from a Tunnel Study with a Photoacoustic Trace Gas Detection System', *Environ. Sci. Technol.*, **30**, 2864–2867 (1996).
79. H.S.M. De Vries, M.A.J. Wasono, F.J.M. Harren, E.J. Woltering, H.C.P.M. van der Valk, J. Reuss, 'Ethylene and CO_2 Emission Rates and Pathways in Harvested Fruits Investigated, in situ, by Laser Photothermal Deflection and Photoacoustic Techniques', *Postharvest Biol. Technol.*, **8**, 1–10 (1996).
80. H. Zuckermann, F.J.M. Harren, J. Reuss, D.H. Parker, 'Dynamics of Acetaldehyde Production During Anoxia and Post-anoxia in Red Bell Pepper Studied by Photoacoustic Techniques', *Plant Physiol.*, **113**, 925–932 (1997).
81. L.S. Monk, R. Brändle, R.M.M. Crawford, 'Catalase Activity and Post-anoxic Injury in Monocotyledonous Species', *J. Exp. Bot.*, **38**, 233–246 (1987).
82. J. Oomens, H. Zuckermann, S. Persijn, D.H. Parker, F.J.M. Harren, 'CO-laser Based Photoacoustic Trace Gas Detection; Applications in Postharvest Physiology', *Appl. Phys. B*, **67**, 459–466 (1998).
83. W. Armstrong, R. Brändle, M.B. Jackson, 'Mechanisms of Flood Tolerance in Plants', *Acta Bot. Neerl.*, **43**, 307–358 (1994).
84. M.B. Jackson, 'Rice for Life: A Physiological Basis for Improving Submergence Tolerance in Rainfed Lowland Rice', First Annual Progress Report, European Commission INCO-DC, Contract: IC18-CT96-00078, 1998.
85. A. Singh, K.B. Evensen, T. Kao, 'Ethylene Synthesis and Floral Senescence following Compatible and Incompatible Pollinations in *Petunia inflata*', *Plant Physiol.*, **99**, 38–45, 1992.

86. T. Kuboyama, C.S. Chung, G. Takeda, 'The Diversity of Interspecific Pollen-pistil Incongruity in *Nicotiana*', *Sex. Plant Reprod.*, **7**, 250–258 (1994).
87. J.M. Lepponen, A. Niemi, I. Rinne, 'Nitrogen Fixation of Cyanobacteria (Blue-Green Algae) and the Nitrogen Cycle of the Baltic Sea', *Symbiosis*, **6**, 181–194 (1988).
88. E. Flores, A. Herrero, 'Assimilatory Nitrogen Metabolism and Its Regulation', in *The Molecular Biology of Cyanobacteria*, ed. D.A. Bryant, Kluwer Academic Publishers, Dordrecht, 487–517, 1994.
89. B. Bergman, J.R. Gallon, A.N. Ray, L.J. Stal, 'N_2 Fixation by Non-heterocystous Cyanobacteria', *FEMS Microbiol. Rev.*, **19**, 139–185 (1997).
90. C.P. Wolk, A. Ernst, J. Elhai, 'Heterocyst Metabolism and Development' in *The Molecular Biology of Cyanobacteria*, ed. D.A. Bryant, Kluwer Academic Publishers, Dordrecht, 769–823, 1994.
91. R.W.F. Hardy, R.D. Holsten, E.K. Jackson, R.C. Burns, 'The Acetylene–Ethylene Assay for N_2 Fixation: Laboratory and Field Evaluation', *Plant Physiol.*, **43**, 1185–1207 (1968).
92. R.J. Flett, R.D. Hamilton, N.E.R. Campbell, 'Aquatic Acetylene-reduction Techniques: Solutions to Several Problems', *Can. J. Microbiol.*, **22**, 43–51 (1975).
93. A. Haystead, R. Robinson, W.D.P. Stewart, 'Nitrogenase Activity in Extracts of Heterocystous and Non-heterocystous Blue-Green Algae', *Arch. Mikrobiol.*, **74**, 235–243 (1970).
94. H. Zuckermann, M. Staal, L.J. Stal, J. Reuss, S. te Lintel Hekkert, F.J.M. Harren, D.H. Parker, 'On Line Monitoring of Nitrogenase Activity in Cyanobacteria by Sensitive Laser Photoacoustic Detection of Ethylene', *Appl. Environ. Microbiol.*, **63**, 4243–4251 (1997).
95. M.O. Andreae, 'Ocean–Atmosphere Interactions in the Global Biogeochemical Sulfur Cycle', *Mar. Chem.*, **30**, 1–29 (1990).
96. T.S. Bates, B.K. Lamb, 'Natural Sulfur Emissions to the Atmosphere of the Continental United States', *Glob. Biogeochem. Cyc.*, **6**, 431–436 (1992).
97. M. Philips, 'Breath Tests in Medicine', *Sci. Am.*, July, 52–57 (1992).
98. B. Krotozinsky, G. Gabriel, H. O'Niell, 'Characterization of Human Expired Air: A Promising Investigative and Diagnostic Technique', *J. Chromatogr. Sci.*, **15**, 239–244 (1977).
99. H. Esterbauer, 'Estimation of Peroxidative Damage. A Critical Review', *Pathol. Biol.*, **44**, 25–28 (1996).
100. C.M.F. Kneepkens, G. Lepage, C.C. Roy, 'The Potential of the Hydrocarbon Breath Test as a Measure of Lipid Peroxidation', *Free Radical Biol. & Med.*, **17**, 127–160 (1994).
101. F.R. de Gruijl, 'Health Effects from Solar UV Radiation', *Radiat. Prot. Dosim.*, **72**, 177–196 (1997).
102. A. van Gossum, J. Decuyper, 'Breath Alkanes as an Index of Lipid Peroxidation', *Eur. Respir. J.*, **2**, 787–791 (1989).
103. J.E. Rogers, W.B. Whitman, *Microbial Production and Consumption of Greenhouse Gases*, American Society for Microbiology, Washington DC, USA, 7–38, 1991.
104. J.H.P. Hackstein, C.K. Stumm, 'Methane Production in Terrestrial Arthropods', *Proc. Natl. Acad. Sci.*, USA, **91**, 5441–5445 (1994).
105. P. Kestler, *Comparative Biochemistry and Physiology of Insects*, ed. K.H. Hoffmann, Springer Verlag, Berlin, 137–183, 1985.
106. M.C. Quinlan, N.F. Hadley, 'New System for Concurrent Measurement of Respiration and Water Loss in Arthropods', *J. Exp. Zool.*, **222**, 255–263 (1982).
107. J.R.B. Lighton, D. Garrigan, F.D. Duncan, R.A. Johnson, 'Respiratory Water Loss During Discontinuous Ventilation in Queens of the Harvester Ant *Pogonomyrmex Rugosus*', *J. Exp Biol.*, **179**, 233–244 (1993).
108. E.B. Edney, *Water Balance in Land Arthropods*, Springer Verlag, New York, 227–238, 1977.
109. C.P. Rinsland, E. Mahieu, R. Zander, M.R. Gunson, R.J. Salawitch, A.Y. Chang, A. Goldman, M.C. Abrams, M.M. Abbas, M.J. Newchurch, F.W. Irion, 'Trends of OCS, HCN, SF_6, $CHClF_2$ (HCFC-22) in the Lower Stratosphere from 1985 and 1994 Atmospheric Trace Molecule Spectroscopy Experiment Measurements near 30°N Latitude', *Geophys. Res. Lett.*, **23**, 2349–2352 (1996).
110. S. Svanberg, 'Environmental Monitoring Using Optical Techniques', in *Applied Laser Spectroscopy*, eds. W. Demtröder, M. Inguscio, Plenum, New York, 417–434, 1991.
111 A. Campargue, F. Stoeckel, M. Chenevier, 'High-sensitivity Intracavity Laser Spectroscopy – Applications to the Study of Overtone Transitions in the Visible Range', *Spectrochim. Acta Rev.*, **13**, 69–88 (1990).
112. P. Zalicki, R.N. Zare, 'Cavity Ring-down Spectroscopy for Quantitative Absorption Measurements', *J. Chem. Phys.*, **102**, 2708–2717 (1990).
113. P.O. Wennberg, R.C. Cohen, N.L. Hazen, L.B. Lapson, N.T. Allen, T.F. Hanisco, J.F. Oliver, N.W. Lanham, J.N. Demusz, J.G. Anderson, 'Aircraft-borne, Laser-induced Fluorescence Instrument for the in situ Detection of Hydroxyl and Hydroperoxyl Radicals', *Rev. Sci. Instrum.*, **65**, 1858–1876 (1994).